Bull. geol. Instn Univ. Upsala N. S. 3, 6: 163—200, 1972

THEORETICAL AND EXPERIMENTAL STUDIES OF DIAPIRIC STRUCTURES ON ÖLAND

By

Ove Stephansson

Institute of Geology, University of Uppsala
Box 555, S-75122 Uppsala, Sweden

(Submitted January 24, 1972)

CONTENTS

REVIEW OF DIAPIRIC STRUCTURES IN CLASTIC SEDIMENTS 164
FACTORS WHICH DETERMINE THE CHARACTERISTICS OF DIAPIRS 165
Density ratio of source layer to overburden
Apparent viscosity ratio of source layer to overburden 166
Thickness ratio of source layer to overburden 166
Strength of the overburden 166
Areal extent of source layer 166
Sedimentary history 167
Effective confining pressure and temperature 168
Tectonic activity 168
THE PHYSICAL ARGUMENTS FOR GRAVITY FORMATION OF THE RIDGES AND DOMES OF THE ISLAND OF ÖLAND 169
Measurements of rock density 169
Changes in density 170
Survey of creep properties and viscosity . . 172
THEORETICAL STUDIES 174
Growth of the main ridges on southern Öland 175
Small-scale doming in beds of limestone and marl 177
Formation of diapirs in a multi-layered sequence 179
MODEL EXPERIMENTS STUDIED BY THE CENTRIFUGE TECHNIQUE 181
Initiation of diapirs 181
Irregularities and discontinuities in the source layer 182
Irregularities and discontinuities in the overburden 185
Irregularities and discontinuities in the substratum 188
The influence of jointing and faulting on the initiation of diapirs 191
Model of the Mossberga Dome 192
Models with brittle fracturing 195

ABSTRACT

This paper is a sequal to the author's article 'Gravity tectonics on Öland'. It deals with theoretical and experimental investigations of diapirism with special reference to the different types of diapiric structures found on the island of Öland in southern Sweden.

A review of diapiric structures in clastic sediments is followed by a discussion of the main factors that determine the characteristics of diapirs, including density, viscosity and thickness ratios between buoyant layer and overburden, sedimentary history and tectonic activity. Results of density measurements show the alum shales to have a mean density of 2.32 g/cm^3 and the overlying limestone a mean density of 2.70 g/cm^3. This inverted density stratification gives rise to a gravitational instability that is the driving agency in the formation of the large domes and ridges on southern Öland. The same mechanism is thought to be responsible also for the formation of intermediate and small domes and ridges. In these cases the present density contrast between limestone and marly or shaly intercalations is around 0.12 g/cm^3. As cementation and lithification are ac-

complished more rapidly in carbonate sediments than in other sediments we may assume a preserved density contrast throughout geologic time.

The thickness of limestone required to generate the structure of a main ridge is calculated from theory of gravity instability. For a ridge with a wavelength of 300 m the theory gives a limestone thickness of about 80 m at the time of formation. The bent limestone layers of the small domes and ridges found on Öland have wavelength-thickness ratios which often exceed 6—10. To obtain these values the theoretical results necessitate large viscosity contrasts between the overburden of limestone and the buoyant layer of marl. This result lends support to the idea that the limestone layer was lithified at the time of diapiric growth.

In order to arrive at proper wavelength-thickness ratios in applying the theory for the formation of domes and ridges of multi-layer anticlinal type described in Stephansson (1971b) we have to use viscosity contrasts of the order of 10^6—10^7 for limestone to marl.

The centrifuge method has been used for an experimental study of diapirism. Initiation of diapirs from irregularities and discontinuities in substratum, source layer and overburden is reproduced in models of silicone putty, painter's putty and modelling clay. A model of the Mossberga Dome is analysed and the time required for evolution of this structure is calculated from scale-model theory.

Brittle fracturing accompanying plastic deformation is demonstrated in centrifuged layered models of wax, brittle plates of plaster and painter's putty.

REVIEW OF DIAPIRIC STRUCTURES IN CLASTIC SEDIMENTS

Diapirism, in the broad sense, is defined as a process in which earth materials from deeper levels have pierced, or appear to have pierced, materials at shallower levels (O'Brien, 1968). Normally, diapirism in this broad sense includes igneous intrusion or extrusion and diapirism in the restricted sense (*sensu stricto*). In this paper we shall be concerned with diapirism *sensu stricto*, i.e. the physical emplacement at low temperatures of mostly clastic sedimentary material. From the literature we know that low density evaporites such as halite, carnallite, sylvite, gypsum and anhydrite are common diapiric materials, but we also find non-evaporitic materials such as shale, marl, coal, peat, mud and clay diapiric structures. The chief characteristic of all these materials is their plasticity or ability to flow. Another property which is necessary for the emplacement of gravity structures is for the plastic materials to be of low density. A density contrast between buoyant layer and overburden — an inverted density stratification — is the chief requirement of diapirism. Pore-water pressure, lithostatic pressure, sudden changes in porosity and gas pressure are factors also of importance.

Starting with recent diapirism we know that deposition of thick, localized masses of heavier bar sediments directly upon lighter, plastic clays leads to a gravity instability which may be relieved by diapiric intrusion of the clay. The result is the formation of mudlumps or mud volcanoes. Mud lumps in the Mississippi delta sediments have been investigated by Morgan et al. (1968). From maps dated between 1867 and 1961 the form of the initial mudlumps, their progression outwards from the river mouth and their development cycle have been studied.

According to Freeman (1968) "sedimentary volcanism" would be the term applied to the process by which diapiric clastic rocks are extruded to the surface from great depths as predominantly argillaceous unconsolidated sediments. This term is introduced in order to emphasize the often rapid growth of mudlumps and mud volcanoes in contrast to the slow plastic movement of diapiric materials like salt in salt domes. Mud volcanoes are one of the surface expressions of diapirs and are found in considerable numbers in the island of Trinidad (Suter, 1955, and Higgins & Saunders, 1967).

Piercement structures of clastic material in young mobile belts are a common occurrence. Omara (1964) has investigated a clay-diapir anticline about 10 km west of Cairo in Egypt. This anticline exposes a Cretaceous succession of sandstones, shales, clays and marls along the inner base of its two limbs. The principal shell of the structure consists of Turonian dolomitic limestones. Near the culmination of the warping the incompetent sediments have pierced the anticlinal core and broken out as clay diapirs. A similar structure is described from the Tuscany Zone, west of Bologna in the Apennines (Wiedenmayer, 1950). Here a large anticline in Jurassic and Cretaceous marl and clay with intercalations of salt projects into Younger Miocene rocks. Also, Beloussov (1962, pp. 455—464) mentions several similar structures.

The true diapiric origin of salt structures from places such as the Gulf Coast, Western Germany and Iran was known long ago by many geologists. However, the knowledge of true shale diapirism is rather new. In the Gulf Coast area there are diapiric "shale masses" which differ distinctively from the surrounding sand-shale sequences by possessing low properties of sound velocity transmission, low density, low resistivity and high fluid pressure. These somewhat anomalous properties from the normal situation are caused by high porosity and low permeability of the sediments. The low density shale masses — density slightly less than the density of salt beds — are sometimes associated with salt domes but also form *pure shale diapirs.* The critical prerequisite of their occurrence is thought to be the absence of porous and permeable sediments whose pores are pressure-connected with the atmosphere. Shale diapirs in the Gulf Coast area have been investigated by Atwater (1967), Gilreat (1968) and Musgrave & Hicks (1968).

Dome cores which consist of diapiric salt and shale are rather common structures in the salt-dome area of south Lousiana (Atwater & Forman, 1959). Here the diapiric shale is interpreted as having breached the overlying sediments, and sometimes the shale component of the dome core has risen higher than the salt. This in fact shows the intrusive nature of the shale and demonstrates that it has not just been dragged upward by the intrusive salt.

During the past decade, seismic reflection profiling has revealed diapiric structures beneath many continental margins and adjacent deep-sea areas. The structures are abundant in marginal oceanic basins such as the Mediterranean Sea (Watson & Johnson, 1968); the Gulf of Mexico (Burk et al., 1969); and the Pacific continental margin (Bennet, 1969). In addition intrusive plugs of shale have been discovered in the south-eastern Bering Sea (Scholl & Marlow, 1970).

Unconsolidated, water-saturated sediments are subjected to various small deformations which may start with, or shortly after, deposition. These deformations are mostly caused by load effects due to gravity. Some of the resulting structures have been described as "flow casts" (Schrock, 1948); "load casts" (Kuenen, 1953) and "load folds" (Sullwold, 1959). Deformational sedimentary structures characterized by crumpled and irregular bedding in limestones are explained as being due to instability in density stratification (Bogacz et al., 1968). The same explanation is given to the small domes and ridges in the Lower Ordovician limestones of Öland, southern Sweden (Stephansson, 1971b). Many investigators of flysch, deltaic and occasionally fluviatile deposits mention in their writings sediment injection structures such as sand dykes (Dzulynski & Walton, 1965); sediment pipes (Friend, 1965); sand volcanoes (Gill & Kuenen, 1958). These structures are discussed from a diagenetic point of view by Swarbrick (1968) and Daley (1971) and some of them have been reproduced experimentally by Graff-Petersen (1967).

FACTORS WHICH DETERMINE THE CHARACTERISTIC OF DIAPIRS

In principal there are two separate schools of thought concerning the origin of diapiric structures. There are geologists who believe that these structures are developed solely by tangential stresses sometimes in combination with basement faulting and those who believe in the concept of gravitational instability. Here the works of Arrhenius et al. (1912), Nettleton (1934) and Ramberg (1963, 1967) are particularly significant because these authors postulated and also demonstrated experimentally that salt domes can be formed gravitationally due to the lower density of salt in comparison with the overlying sediments. Although most of the diapiric structures originate as a result of gravity instability tectonic processes such as subsidence, uplift, differential movements and faulting before, during or after emplacement are of the greatest importance in determining the final pattern of a diapiric structure. The main factors affecting the development are presented in Fig. 1.

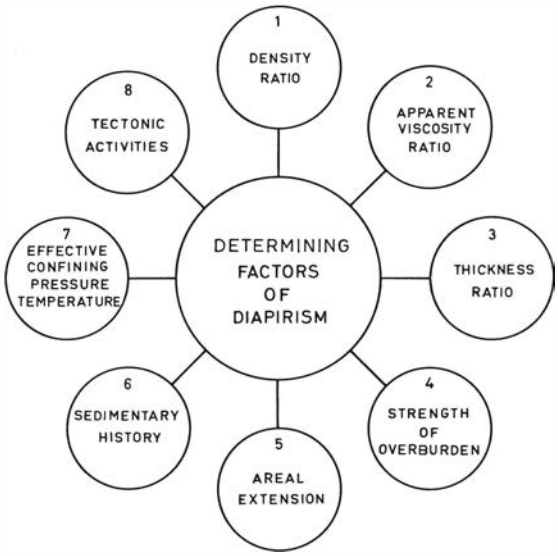

Fig. 1. The most important factors which determine the characteristics of diapirs; a modified figure after O'Brien (1968).

Density ratio of source layer to overburden

The driving power of most diapiric structures is a difference in density between a source layer and the overburden, causing a net drop in the gravity potential (Ramberg, 1967). This gravitational instability is not relieved until the lighter material has moved on top of the overburden, a common situation in sedimentary volcanism when mudlumps and mud volcanoes are formed. In many salt domes and shale domes, with a slow plastic flow, this process of complete inversion is prevented by the strength of the overburden, a progressive drop in density towards the top of the overburden and an increasing apparent viscosity of the buoyant layer towards the surface due to decreasing pressure and temperature.

Apparent viscosity ratio of source layer to overburden

The ratio of apparent viscosity of overburden to buoyant layer is a controlling factor for both time and rate of formation of a diapiric structure. The dimension of the diapir is also controlled by this ratio. Generally, by keeping the apparent viscosity of the overburden constant and varying that of the buoyant layer, we obtain a rapid formation of the diapir with a relatively small areal cross section perpendicular to the flow direction for large ratios. A small ratio, on the other hand, yields a larger cross section but a longer time of formation. This effect has been demonstrated by Ramberg (1967, pp. 54—57) in experimental tests with oil-syrup models.

Thickness ratio of source layer to overburden

We know that the rate of diapiric initiation and formation increases with increasing thickness of the source layer provided all the other parameters are kept constant. This is in full agreement with model laws since the model ratio of velocity is proportional to the square of the model ratio of length, provided the materials involved and the acceleration are kept constant. Hence, theoretically the rate of evolution of diapiric structures increases with the square of the buoyant-layer thickness (Ramberg, op. cit.). As will be demonstrated later, a finite thickness of one or both layers will produce a certain growth of relative amplitude which attains a maximum value at a certain wavelength.

Strength of the overburden

This factor is of major importance in diapiric initiation and emplacement. If the overburden and/or source layer possess a finite yield strength a small irregularity in geometry or material property is necessary to generate diapirism. The buoyant force per unit area of the source layer must exceed the 'plunging strength' of the overburden. At present we really do not know if rock masses possess any definite yield strength at a very slow rate of deformation, because plastic flow — creep — is found at very small values of deviatoric stress. The liquid experiments of Ramberg (1967a) clearly demonstrate that materials with infinitely small yield strength start doming without irregularities other than at the molecular level. If a growing diapir reaches a competent layer with high plunging strength the doming material starts to spread laterally to form a conformable sill underneath the competent layer (Ramberg, 1963, fig. 4).

Areal extent of source layer

The form of the outer boundary of the source layer is a strong controlling factor for the geometry and growth pattern of diapiric structures. In nature we often find diapiric anticlines running more or less parallel with the major axis of an evaporite or sedimentary basin, e.g. the northern Zechstein basin in Germany (Trusheim, 1960) and the Paradox basin at the border of Utah and Colorado, described by Elstone and Shoekmaker (1963). Similar structures are also observed in model experiments; cf. Ramberg (1967a, figs. 12 and 13). The diapir-generating effect is caused by the pressure difference at the edge of the source layer which initiates a horizontal flow of the surrounding material towards the source, and a ridge is produced. The outer boundary effect together with a maximum thickness of the source layer in the centre of the basin often result in the initial formation of diapiric anticlines at the centre. Outwards the anticlines are flanked by single domes and finally pillows, i.e. slightly curved domes with small "amplitudes" (Trusheim, 1960).

Sedimentary history

A wide range of subaqueous sedimentary structures have been classified according to the behaviour of sediments at the time of formation of the structures and according to the nature of the motions to which these sediments have been subjected at that time. Such a classification, based on rheological and kinematic parameters, have been proposed by Elliot (1965). In his *endokinematic* class, "operations in which the largest displacement to form the structure and the unmodified deposit" (Elliot, op. cit., p. 196), we recognize the diapiric structures. The range of sediment behaviour at emplacement he subdivides into solid, quasi-solid, hydroplastic, quasi-liquid and liquid and these behaviour styles are in turn defined in terms of the freedom of the constituent sedimentary particles. In this scheme a hydroplastic behaviour of a sediment is, according to Elliot, obtained where the particles are so loosely packed that they can revolve somewhat around their neighbours to such a degree that the whole mass can change shape and yet are so confined or cohesive that they cannot change their neighbours. Elliot refers small diapiric folds to hydroplastic sediment behaviour and mudlumps to the transition hydroplastic — quasi-solid behaviour.

Swarbrick (1968, p. 165) classifies intrusive sediments into two major classes: "(a) those which involve the injection of plastic or hydroplastic sediments; (b) those involving the intrusion of liquid sediments". The main distinction between them is the state of gelation of colloidal sediment, and the water content of granular sediment.

In all sedimentary structures due to gravity the dominant factor determining the properties of the sediments is the amount of water in the sediment, but the pressure to which that water is subjected is also of importance. Following the reasoning of Swarbrick (op cit.) we know that sediments initially contain 60 % and 80 % water and that most of it fills the pore spaces. Further, that the activity arising from this water content changes with increasing depth in the sediment pile. In granular sediments at shallow depths the low hydrostatic pressure allows grain-to-grain contact and thus the sediment retains a certain shear strength. The high water content in an argillaceous sediment makes it essentially "liquid" with very low shear strength. The pore pressure rises in both types of sediment with increasing depth and at a critical depth the pore pressure can equal the lithostatic pressure and the shear strength is reduced almost to zero. At levels above this, granular sediments with a small clay component may flow hydroplastically and addition of a small amount of water to these sediments will allow them more freedom and a liquid behaviour according to Swarbrick.

The pore pressure and water content are also of great significance in lowering the strength and retaining a low density of a rock mass after lithification has occurred. Whenever the pore pressure is normal (not exceeding about 0.5 of the overburden pressure) the sediment must in effect be coupled to the atmosphere through a permeable conduit so that attainment of hydrostatic pressure is possible. Any system with abnormal formation pressure is not in equilibrium and, hence, must be isolated by some kind of an impermeable barrier. The most common cause of this high formation pressure is a rapid deposition of impermeable, fine-grained sediments which become undercompacted due to unexpelled connate water. According to Handin (1968) the pressure can also rise by simple deformation of the pores if the fluid can not espace, or as a result of a tectonic activity where an isolated element of a rock could be placed in a position where its interstitial pressure would exceed the normal pressure of the surrounding rocks. Finally, the water expelled from hydrous minerals when their transition temperature it reached certainly effect the mechanical properties of rocks directly by increasing the pore pressure due to the water expelled. The effect of pore pressure in reducing strength and frictional resistance has been invoked by Hubbert & Rubey (1959) to explain gravity gliding of thrust sheets for distances of many kilometers.

Effective confining pressure and temperature

The behaviour of different stratified rocks during diapiric processes depends upon both relative strength and ductility (for example the strength of a sandstone and a limestone can be almost the same but the ductility and hence the ability to flow uniformly are more favoured in a limestone). Experimental deformation tests have shown that for most sedimentary rocks subjected to constant temperature and strain rate the effective confining pressure raises the yield stress, which favours strain-hardening and ductility. A reduction of ultimate strength, yield stress, and strain-hardening, but increase in plasticity is obtained at a constant confining pressure when temperature is increased at constant strain rate or strain rate is decreased at constant temperature (Griggs & Handin, 1960).

The term effective confining pressure also includes the effect of pore pressure. By increasing the pore pressure the strength and ductility of a rock are reduced. This is not because the cohesive strength or coefficient of internal friction are modified, but simply because all effective normal stresses and, hence, frictional resistance are lowered. Physically the situation is such that the interstitial fluid to some extent supports the weight of the superincumbent material. From the literature we know that ratios of pore pressure to overburden pressure as high as 0.9 have been measured.

The rate of strain and the apparent viscosity of sedimentary rocks are also strongly influenced by temperature and effective confining pressure. Experimental deformation of rocks at different temperatures and pressures led Heard (1968) to propose the following relationship

$$\dot{\varepsilon} = A\, exp(-E/RT)\, \sigma^N$$

i.e. a thermally activated process where $\dot{\varepsilon}$ is the rate of strain, E the activation energy, T absolute temperature, σ stress, and A, R, N material constants. The apparent viscosity is now obtained from the equation

$$\eta = \frac{\sigma}{3\dot{\varepsilon}}$$

Tectonic activity

In any theory of the genesis of diapiric structures, geologists have searched for some mechanism that would initiate the upward growth of the diapir. Irregularities in the basement rock beneath the source layer or in the upper surface of that bed, basement rock movements, variation in thickness or composition of the overburden and, finally, all types of faulting have been proposed. As a result of model studies Parker and McDowell (1955) have suggested that (1) variation in thickness of overburden and (2) faulting appear to be the most probable causes of initiation of salt domes. The position of salt ridges, as well as of groups of individual salt domes which have a pronounced regional alignment may in some part have been governed by regional flexures.

The initiation of diapiric growth along a fault zone is mechanically easy to understand. Suppose we have an ordinary dip-slip fault where some vertical movement of the blocks has occurred so that the top of the lighter source layer is situated at different levels. At the trunkated edge close to the top of the "upthrown" source layer there is a rapid change in the weight of the overburden which creates a pressure difference on both sides of the fault plane. A similar pressure difference exists at the trunkated edge of the "downthrown" source layer. These differences in pressure yield a horizontal flow of adjacent material towards the source layer together with a vertical flow due to the lower strength of the overburden along the fault. We know that when failure of brittle and semi-brittle rocks takes place great amounts of energy are released and failure completely alters the stress field which initiated the fracturing. Such an energy release and alteration of stress field may be enough for diapiric initiation.

When the diapiric growth of an originally flat-lying bed has started the steadily increasing tensile stresses at the top of the overburden result in tension and failure at the crest. In the case of circular or slightly elongate domes or stocks we often observe a radial faulting in the initial stage followed by peripheral or tangential faulting.

As diapiric material flows plastically into a growing structure it leaves behind a peripheral area of less thickness than the original bed — a rim syncline or "primary peripheral sink" — which results in a structural sag of the piercement layer and the overburden. This structure develops at an early stage of the diapirism and becomes progressively accentuated during growth. As the accumulation of piercement material continues, it eventually causes the overburden to break at the top of the structure and the diapir rises. At the same time the surrounding strata subside, now causing the formation of a new rim syncline, the so-called "secondary peripheral sink". In the development of single salt domes deposition of new sediments is characteristically thickest close to the salt dome in the secondary peripheral sink while it becomes thinnest close to the dome in the primary peripheral sink. This difference in thickness of sediments around a dome led Sanneman (1963) to reconstruct the historical development of salt stocks in northwestern Germany with the aid of refraction-seismic surveys.

THE PHYSICAL ARGUMENTS FOR GRAVITY FORMATION OF THE RIDGES AND DOMES ON THE ISLAND OF ÖLAND

Measurements of rock density

Results of more than one thousand density measurements from the core of a borehole drilled at Segerstad, southern Öland, are presented in Table I. The original values were kindly placed at my disposal by Dr. B. Dahlman of the Geological Survey of Sweden. From the column of mean values we notice that dense Lower Ordovician

Table I. *Rock densities from the borehole at Segerstad, Southern Öland.*

Rock type	Number of measurements	Maximum value	Minimum value	Mean value	Standard deviation	Standard error of the mean
Lower Ordovician Limestones	100	2.76	2.56	*2.69*	0.03	0.003
Lower Ordovician and Upper Cambrian Alum Shales	95	2.50	2.23	*2.32*	0.04	0.004
Middle Cambrian *Paradoxides Paradoxissimus* Beds	192	2.71	2.39	*2.60*	0.03	0.002
Middle Cambrian *Eccaparadoxides Oelandicus* Beds	121	2.72	2.59	*2.62*	0.02	0.002
Lower Cambrian Sandstones	545	2.76	2.20	*2.57*	0.07	0.007

limestones, $\varrho_{mv} = 2.69$ g/cm^3, overlie much less dense Lower Ordovician and Upper Cambrian Alum shales, $\varrho_{mv} = 2.32$ g/cm^3. This inverted density stratification is the main evidence for supposing that a gravity instability led to the formation of the so-called main ridges and large domes on southern Öland (Stephansson, 1971b, pp. 48, 59).

The contrast in density between the Ordovician limestones and the Middle Cambrian silty and shaly beds is thought to have been the driving agency in the formation of the Mossberga Dome on central Öland (Stephansson, op. cit., p. 67). The non-ductile, competent behaviour of the Lower Cambrian Sandstone eliminates the possibility of this rock being a source layer in a process of gravity tectonics, although the mean value of density for this rock is slightly less than that of the Middle Cambrian beds. The very slight bulging of the sandstone below the trunk of the Mossberga Dome could possibly have appeared during the growth of the dome.

More than twenty density measurements of shaly and marly intercalations in the Lower Ordovician limestone sequence have a mean value of 2.57 g/cm^3 ($\sigma = 0.03$ g/cm^3). Several specimens were impure and contained various amounts of limestone. A *present density contrast* of 0.12 g/cm^3 between the pure limestones and the marly and shale intercalations indicates the possibility that gravitational forces caused the medium and small diapiric structures on Öland; cf. Stephansson (1971 b). A theory of gravitational origin of these structures needs, however, to take into account possible changes in density contrast since the time of their formation.

Changes in density

The density of sedimentary rocks is intimately related to most of the processes that constitute diagenesis, i.e. compaction, cementation, formation of new minerals, redistribution and recrystallization. Of great importance in determining density of sedimentary rocks is compaction which is closely related to the parameters porosity and permeability.

The compaction of argillaceous sediments can be directly or indirectly observed in many areas with a young sediment cover. A collection of results from detailed studies on the compaction of argillaceous sediments is presented in Fig. 2. The porosity-depth relationship is based on measurements made by Athy, Hedberg and Dickinson taken from Rubey & Hubbert (1959, fig. 2) and measurements by Storer and von Engelhardt taken from von Engelhardt (1960, fig. 20). As shown in the figure a relation exists between the logarithm of the porosity and depth, with fairly good accuracy for depths greater than about 100 m. This can be expressed by the empirical equation:

$$\varepsilon = \varepsilon_0 A^{-z} \qquad (1)$$

where ε is the porosity at a depth z, ε_0 the apparent porosity at $z = 0$ (notice that the absolute porosity close to the surface is often as high as 70—80 % in recent clay-rich sediments). A is a constant and z is depth in thousands of metres. The constants calculated from the curves in Fig. 2 are presented in Table II. The fact that the porosity depth curve 5, based on Dickinson's data for the Gulf Coast area, shows higher porosities than the curve for other regions is probably to be explained by the common occurrence of abnormally high fluid pressure there. The porosity-depth relationship of steep negative slope obtained by Athy for sedimentary rocks of Oklahoma, curve 1, may be due to the fact that the samples were taken from areas of strong deformation and, hence, some of the compaction may have resulted from tectonic stresses. The three curves situated between the two extremes probably represent fairly well the porosity-depth relations of an average shale or mudstone in a tectonically undisturbed area. Deviations from the empirical relationship (equation 1) occur for small depth but may occur for great depth.

Although no available data exist regarding the porosity-depth relationships for carbonate sediments, except for a very few observations of lime mud, "it is important to note that cementation and lithification of carbonate sediments is accomplished more rapidly than that of other sediments" (Larsen & Chillinger, 1967, p. 7). Hence, the gradient of decreasing porosity with depth

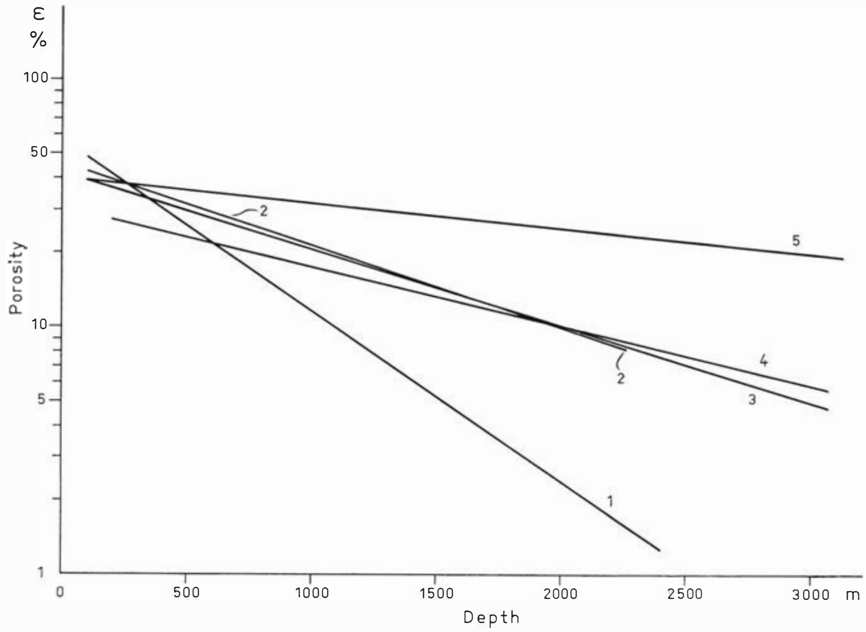

Fig. 2. Porosity versus depth for argillaceous sediments; the original values are taken from Rubey and Hubbert, 1959, and von Engelhardt, 1960.

will be much steeper for carbonate sediments than for argillaceous sediments; cf. Fig. 2.

The degree of compaction of a sediment whose pore space is considered to be filled with water or any other solution with constant density, may be inferred from the bulk density which in turn is related to porosity by the equation

$$\varrho_b = \varrho_g - (\varrho_g - \varrho_w) \cdot \varepsilon \qquad (2)$$

where ϱ_b is the bulk density at fluid saturation and ϱ_g and ϱ_w are the grain and water/solution densities respectively. ε is the porosity. This equation simply shows that the bulk density ϱ_b varies linearly from that of water or solution when the porosity is 1 to that of the mineral or grain density ϱ_g when the porosity is zero. A combination of eqs. (1) and (2) yields the relationship between bulk density and depth which is of importance in the theoretical calculations and the scale model experiments.

Table II. *Constants calculated from the curves in Fig. 2.*

Sediment	ε_o	A
1 Permian, Oklahoma (Athy)	58	0.20
2 Tertiary, Venezuela (Hedberg)	46	0.45
3 Tertiary, Po Basin (Storer)	43	0.48
4 Liassic, NW-Grmany (von Engelhardt)	31	0.57
5 Tertiary, Gulf Coast region (Dickinson)	28	0.78

The two curves in Fig. 3 are graphical representations of equation (2) for the Ordovician limestones and the alum shales. One end of each curve is determined by the unit density ($\varrho_w = 1$) at 100 % porosity. The slope of the curves are obtained after plotting the present mean densities and porosities of the rocks. Values of density were taken for the borehole at Segerstad (cf. Table I) whereas the porosity values were derived for the same lithological units for the borehole at Böda Hamn (Hessland, 1955). The numbers in Fig. 3 correspond to: 1, Ordovician limestones; 2, Alum shales; 3, *Eccaparadoxides Oelandicus* Beds; and 4, Lower Cambrian Sandstone. From the appearance of the two curves we may assume that the

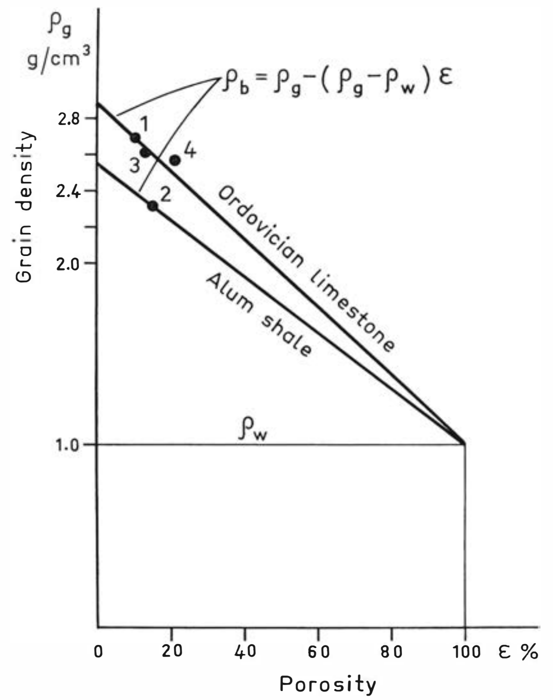

Fig. 3. Bulk density of Ordovician limestone and Alum shale in relation to grain density and porosity; measured density and porosity of: 1, Ordovician Limestones; 2, Alum shales; 3, *Oelandicus* Beds; 4, Lower Cambrian Sandstone. The density values are taken from the borehole at Segerstad, Table I, and the porosity values from corresponding units at the Böda Hamn boring, Hessland (1955).

rocks have possessed a density contrast throughout the diagenetic process. It does not seem very likely that the two curves would cross, because lithification and hence decrease in porosity take place more rapidly in the limestone.

Density values for the *Paradoxissimus* Beds and the Lower Cambrian Sandstone plot very close to the curve for the Ordovician limestone. A density contrast between the limestone and the two other rock types is retained because of the smaller porosity of the limestone. Argillaceous shales and marls are also supposed to have acted as buoyant layers in the formation of diapiric structures, e.g. the small domes and ridges (Stephansson, 1971b). As cementation and lithification in carbonate sediments are accomplished more rapidly than in other sediments we may assume density ratios of 0.90 to 0.95 for the *Paradoxissimus* Beds and the limestones and marl or shale intercalations and the limestones respectively.

Survey of creep properties and viscosity

Having discussed the requirement of low density the second main characteristic of a diapiric material is its plasticity, i.e. its ability to flow. The slow, time-dependent deformation of solid material under the influence of deviatoric stress is called creep. Rock creep is exceedingly complex and is a function of temperature, confining pressure, stress, time etc. By loading a specimen of rock it becomes apparent that four stages of deformation can be distinguished three of which are time dependent

- — instantaneous elastic deformation
- — primary or transient creep in which the rate of creep decreases continuously with time (exponentially or logarithmically)
- — secondary creep or steady-state creep with a a constant rate of creep
- — tertiary or accelerating creep in which the creep rate increases until the experiment is terminated by rupture.

Several empirical equations have been proposed for the different types of creep; cf. Stephansson (1967).

The elastic, plastic and time-dependent properties of rocks under various methods of loading can be described in terms of so-called rheological models, which are composed of combinations of springs, dashpots and sliding blocks. A review of different rheological models hitherto used to describe the behaviour of sedimentary rocks has been given by Stephansson (op. cit.). From this investigation and from measurements of deformation of sedimentary rocks made by Price (1966), Kidybinski (1966) and Hardy (1959) we know that most of these rocks exhibit rheological properties in accordance with a viscoelastic plastic Burgers substance.

Steady-state creep is almost certainly the most significant stage of creep in naturally deforming rocks. In rocks which have been flowing for a long interval of time primary creep cannot be expected to have contributed much to the total deforma-

Table III. *Summary of viscosity data.*

ROCK TYPE	VISCOSITY Poises	SOURCE	METHOD	REMARKS
Limestone	$2 \cdot 10^{19}$	Nettleton	Sagging beam	
Limestone	$1.2 \cdot 10^{18}$	Bingham Odé (1966)	Sagging beam	
Limestone	$1.3 \cdot 10^{18}$	Hubbert		
Warsop nodular Limestone	$1 \cdot 10^{18}$	Price (1964)	Sagging beam	Steady-state creep
Solenhofen Limestone	$1.3 \cdot 10^{15}$	Griggs (1936)	Triaxial test	Unjacketed specimen 10 kbs. confining pressure 5.4 kbs. diff. pressure, room temp.
Solenhofen Limestone	$2 \cdot 10^{22}$	Griggs (1939)	Creep test	Transient creep $= 2 \cdot 10^{14}$ sec^{-1} under normal p-T conditions
Bituminous coal	$10^{16} - 10^{17}$	(Pomeroy) Odé (1966)	Constant loaded contilever beam	Transient creep
Bituminous coal	10^{17}	Morgans and Terry (1958)	Creep test	From the secondary creep of a simple visco-elastic Burgers model
Cannel coal	$6 \cdot 10^{17}$ $2 \cdot 10^{16}$	Kidybinski (1966)	Sagging beam	Steady-state creep Transient creep
Mudstone	$8 \cdot 10^{16}$	Kidybinski (1966)	Sagging beam	Transient creep
Calcareous silstone	$1.1 \cdot 10^{16} - 4.7 \cdot 10^{16}$	Price (1964)	Sagging beam	Steady-state creep
Bearpaw shale	10^{14}	Casagrande et al.	Creep test	23.7 % water at the end of the test
Umeda Alluvial Clay	$2 \cdot 10^{11}$	Murayama and Shibate	Uniaxial compression	65 % water content
Illite Clay	$2.6 \cdot 10^{13} - 1.3 \cdot 10^{14}$	Tan Odé (1966)	Torsion plastometer	45 % water content
Clay	$3.3 \cdot 10^{12}$	Lara-Thomas	Torsion plastometer	20 % water content
Clay	$3.6 \cdot 10^{5}$	Russel	Compression at	34.9 %
	$0.9 \cdot 10^{6}$	and Hanks	constant rate of	26.8 % water content
	$1.8 \cdot 10^{6}$		strain $= 10^{-1} sec^{-1}$	24.2 %

tion. As the flow of sedimentary rocks is assumed to take place by steady-state creep the equivalent viscosity can be estimated once the deviatoric stress σ^l and rate of strain $\dot{\varepsilon}^l$ are known.

$$\eta_a = \frac{\sigma^l}{3\dot{\varepsilon}^l}$$

Since apparent viscosity is a function of applied stress, temperature and confining pressure it is non-linear, and so this equation is valid only for certain values of σ^l and $\dot{\varepsilon}^l$. Viscosity data for rocks which are of the same or almost the same type as those found on Öland are listed in Table III. Several values are taken from a comprehensive summary of viscosity data presented by Odé (1966). The author fully agrees with the statement stressed by Odé that "at this moment, it is impossible to state with confidence the equivalent viscosity of any rock under geologically realistic conditions" (op. cit., p. 53). However, there is no doubt that the data available give some indication of the relative viscosities of different types of rock.

From several creep investigations we know that increasing confining pressure and temperature both lower the apparent viscosity of rocks; cf. Griggs' results in Table III. It is also known that most viscosity data from laboratory experiments are obtained at rates of strain that are too high in comparison with what is to be expected for slow, plastic flow in the upper part of the Earth's crust. Estimating apparent viscosity according to the equation for a rock deformed under normal pressure and temperature conditions but at geological rates of strain, would give larger values than if the rock was deformed in the laboratory. Accordingly, there is a tendency for an increasing viscosity due to a decreasing strain rate to be compensated for by a lowering in viscosity due to increasing temperature and confining pressure.

Although the viscosities of the Öland rocks at the time of diapiric movements are unknown the apparent values obtained experimentally from different investigations of similar rocks are of great value, because they allow an estimation of relative viscosities between different layers in a layered rock sequence. Table III gives a summary of viscosity data from different investigators. Except for the data taken from Griggs (1936, 1939), the mean value of apparent viscosity for limestone is found to be around $5 \cdot 10^{18}$ poises. No viscosity data exist for alum shale at present, and very few are available for shales. Bituminous coal, mudstone and calcareous siltstone have a mean viscosity in the range of $10^{16} - 10^{17}$ poises. The very plastic behaviour of alum shale is evident from present borings in Scania, southern Sweden, where large plastic flow has been measured in the drill holes (Tallbacka, personal communications). The values $5 \cdot 10^{18}$ poises for Ordovician limestones, $5 \cdot 10^{16}$ poises for alum shales and $5 \cdot 10^{17}$ poises for *Paradoxissimus* and *Oelandicus* Beds have been used in the theoretical calculations and scale model work in simulating the formation of the main ridge and large dome structures on southern Öland.

Some viscosity values for clays are also presented in Table III. Here we notice the rapid increase in viscosity with decreasing water content. Some of these values have been used in the calculations for the very early formed small domes and ridges.

THEORETICAL STUDIES OF DIAPIRISM

Recent results from theoretical studies of layered systems in the field of gravity make it possible to determine the dominant wavelength and the rate of growth during the early stage of evolution of a light viscous layer buried below a more dense viscous overburden (Biot & Odé, 1965, and Ramberg, 1967, 1968a, b). A full treatment of the theory used in this article is presented in Ramberg (1968a, b).

The physical model consists of horizontal layers that are welded together. Each layer is uniform in density, viscosity and thickness. If a stack of layers is gravitationally unstable, i.e. it contains layers that are less dense than overlying layers, such a system tends to develop gentle waves with a wavelength characteristic for the particular system. The waves gradually form ridges which tend to split up into individual domes in the course of their rise. For most systems it is found that the rate of upward growth assumes a maximum value at a certain wavelength which is characteristic for the given system. This wavelength which in the course of time will dominate the dynamic evolution of the system is called the *dominant wavelength.*

According to Ramberg (1972) the mathematical analysis leads to the following equation for the rate of growth of amplitude of the waves at the different interfaces

$$[v_j] = [k_{ji} q_{i:1}] \, [q_1 y_i] \qquad (3)$$

where k_{ji} are coefficients determined by the ratios between the thicknesses and viscosities of the layers and the ratio between the thicknesses and the wavelength symbolized by $\varphi_i \equiv 2\pi \dfrac{h_i}{\lambda}$.
$q_i \equiv \frac{1}{2}(\varrho_i - \varrho_{(i+1)}) h_{(i+1)} \cdot g \cdot \mu^{-1}_{(i+1)}$ and y_i is the amplitude of the deflections on interface i.

The integrated form of eq. (3) is

$$[y_i] = [c_{ij}] \, [exp(\varkappa_j q_1 t)] \qquad (4)$$

c_{ij} are coefficients determined in part by the dimensionless parameters of the system and in part by the initial amplitudes; $\varkappa_j$ are the eigenvalues of the matrix of coupling coefficients, q_1 is defined above and t is time. The $\varkappa_j$-value which gives the largest positive product $\varkappa_j q_1$ in the exponent yields the largest amplitude in the course of time. In theory the dominant wavelength is determined with the maximum value of $\varkappa$. For practical reasons $\varkappa_1$ is generally considered as a function of φ_2 — i.e. the wavelength in relation to the thickness of layer 2 counted from the top of a multilayer.

For system with more than one flexible interface the rate of amplitude growth on interface i is given by

$$v_i = \varkappa_1 q_1 y_i \qquad (5)$$

and the amplitude (on i) after a time t after integration is

$$y_i = y_{oi} \, exp(\varkappa_1 q_1 t) \qquad (6)$$

where y_{oi} is the initial amplitude of the deflections on interface i.

In several papers by Ramberg (1968a, b; 1972) results for a number of unstable systems have been computed. Below are a few examples of geodynamically relevant systems with application to different diapiric structures on the island of Öland.

Growth of the main ridges on southern Öland

In a previous article Stephansson (1971b) described and classified different types of ridges. One of the ridges, a so-called main ridge of the "single-layer anticlinal diapir" type, crosses the southern part of the Great Alvar on southern Öland. This ridge has a length of almost 30 km and the width varies between 50 m and 300 m. A few hundred metres west of the village of Kvinsgröta on the southeastern border of the Great Alvar the ridge is well exposed and shows the very typical "pinch-and-swell" structure (Stephansson, op. cit., fig. 5).

From drilling for water in this area we know that the Ordovician limestones are about 3 m thick at the crest of the ridge and are of Arenigian age (Billingen Stage according to observations made by Dr. K. Larsson). 500 m east of the crest line the thickness of the limestone is known to be 20 m. From the drillings we also know that

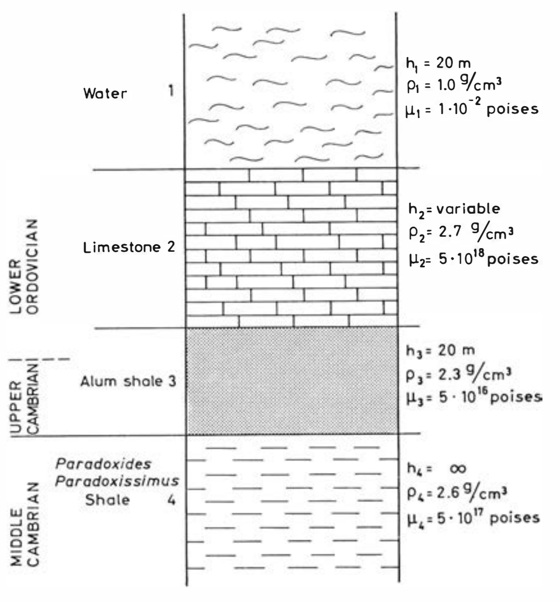

Fig. 4. A model for calculating the thickness of Lower Ordovician Limestone required in order to obtain a main ridge with the dimensions found at Kvinsgröta.

the thicknesses of the underlying alum shales are 33 m thick at the hinge of the structure (below the crest of the ridge) and 17 m thick 500 m east of the ridge. Hence, the closure or amplitude of the ridge is about 16 m, the structure has a width or wavelength of slightly more than 300 m and the rather steeply dipping older limestone beds in the hinge zone are flanked by progressively younger and more gently dipping beds; cf. Stephansson (op. cit., fig. 7).

By using Ramberg's theory we are able to find the thickness of the limestone pile necessary in order to obtain a structure with the dimensions now found at Kvinsgröta. In our model we assume a 20 m thick layer of alum shale resting on a substratum of shale with infinite thickness. The layer of buoyant alum shale ($\varrho_3 = 2.3$ g/cm^3) is overlain by dense limestones ($\varrho_2 = 2.7$ g/cm^3) and 20 m of water of unit density. The model and appropriate thicknesses, densities and viscosities are shown in Fig. 4.

The function $\varkappa_1 = f(\varphi_2)$ has been computed within a region around the maximum for different thickinesses of the limestone layer, h_2, and the results are shown in Fig. 5. We notice how the maximum occurs at larger φ_2-values, or larger values of the dominant wavelength, as the thickness of the limestone layer increases. We know that the width or wavelength of the ridge at Kvinsgröta is slightly more than 300 m. Applying the theory the corresponding limestone thickness will be about 80 m. One assumption made in deriving this is vanishing yield strength and Newtonian properties for the materials. From what we know about the thickness of Ordovician limestones in the Baltic area, e.g. 94 m at File Haidar and 99 m at Visby, both on the island of Gotland, (Thorslund in Magnusson et al., 1962), and an estimated thickness of 80—90 m for Öland (Martinsson, 1958), Lindström, 1971) the thickness required by the theory is quite reasonable.

Although there are uncertainties about the absolute values of densities and viscosities we know that structures having identical corresponding viscosity ratios, thickness ratios and density-contrast ratios will remain geometrically similar during their evolution. According to Ramberg (1968a, eq. 86) it follows that the ratio of viscous force to gravity force is the same for all geometrically similar structures and consequently such structures are also dynamically similar. Hence, the kappa-functions derived for the main ridge at Kvinsgröta are valid for all thickness density and viscosity ratios having the same values as those given in the model shown in Fig. 4.

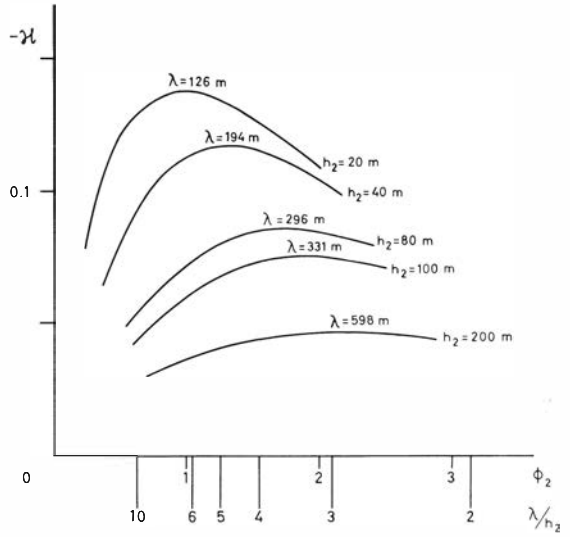

Fig. 5. Kappa-functions for the gravitationally unstable layer of Alum shale for different thicknesses of Lower Ordovician Limestone. The width of the main ridge at Kvinsgröta is around 300 m which corresponds to a limestone thickness of 80 m at the time of ridge formation.

The computed eigenvector that belongs to the maximum value of $\varkappa_1$ for a 80 m thick layer of limestone gives the following proportions between the amplitudes $y_1/y_2/y_3 = 0.137/1.0/0.318$, meaning that the deflection of the surface of the limestone bed should only be 13.7 % of the deflection of the lop of the alum shale layer. To determine the deflection and rate of growth we use the eqs. (5) and (6). From the values $\varrho_1 = 1$ g/cm^3, $\varrho_2 =$

Table IV. *Amplification of deflection of alum shale layer.*

years	10^6	$2 \cdot 10^6$	$5 \cdot 10^6$	10^7	$2 \cdot 10^7$
y_2/y_{02}	37.7	$1.42 \cdot 10^3$	$7.63 \cdot 10^7$	$5.82 \cdot 10^{15}$	$3.39 \cdot 10^{31}$

2.7 g/cm^3, $h_2 = 80$ m, $g = 981$ cm/s^2 and $\mu_2 = 5 \cdot 10^{18}$ poises we obtain $q_1 = -1.34 \cdot 10^{-12}$ sec^{-1}. Insertion of q_1 and $\varkappa_1 = -0.0858$ in eq. (6) gives the ratio between the finite and initial amplitudes at various times (see Table IV). This implies that an initial deflection with amplitude 1.13 cm will grow to the present amplitude, 16 m, after 2 million years. At the moment when the deflection starts to grow ($y_{o2} = 1.13$ cm) the velocity of growth is $v_2 = \varkappa_1 \cdot q_1 \cdot y_{o2} = 0.35$ cm/year. It must be emphasized that these values of amplitude and velocity of growth assume a vanishing yield strength for the material. The effect of yield strength as a possible restraining factor in the growth of the main ridges is evident from their present shape. The rise of the ridges seems to have reached the stage of evolution where a long anticline starts to be unstable and tends to split up into individual domes. At this stage the doming process has ceased. The present position and orientation of the main ridges seem to have been controlled by early tectonically formed weak zones radially diverging from an area just west of the border of the Great Alvar on a level with Mörbylånga (Stephansson, 1971b). These weak zones also seem to have created the necessary initial deflection of the buoyant layer and lowering of strength of the overburden.

Small-scale doming in beds of limestone and marl

The first description of "sedimentary folds" in the Lower Ordovician limestone of Öland was given by Lindström (1963). According to him some tectonic movement was the trigger action that caused limestone beds to glide down a gentle slope to result in folding where beds were pushed together. Later Gidon and Lindström (1965) proposed a mechanism of buckling due to humidity changes and dilatation of the limestone surface to explain some of the structures. Development of the small domes and ridges as a result of the gravitational instability of marl overlain by denser limestone was suggested by Stephansson (1971 b, p. 72). The same mechanism was proposed independently for some of the dome structures by Wamel (1971). He distinguished between "pierce-structures" and "small-scale domes", the former

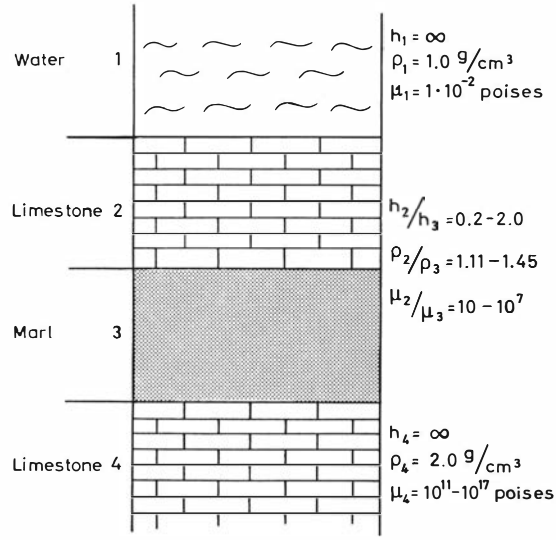

Fig. 6. Model for calculating the dominant wavelength of small ridges and domes for different ratios of thickness, density and viscosity of layers 2 to 3.

term applied where plastic clay (marl) had pierced a layer of hardened limestone, and the latter term applied where the limestone layer is intact and bent upward. Wamel assumes that the bending of this layer was caused by the force of crystallization of calcite, resulting in the development of space under the culmination which was later filled with plastic material. This is where the present author disagrees with Wamel. It will be demonstrated below that there is no need to invoke crystallization forces in order to explain the formation of the small-scale domes and ridges.

In a comment on Wamel's paper, Lindström (1971) accepts the mechanism of gravitational instability in the main but "for other cases of warped bedding, further processes may have been at work in addition to the doming most notably some horizontal sedifluction (sediment creep)", (op. cit., p. 94). The tendency for some of the diapiric structures to be elongated in the direction north-northwest—south-southeast, or perpendicular to the strike of the outcrop, confirms the theory of sedifluction according to Lindström (1971), but can also be explained as due to a "Schnitteffect" or due to existing weak zones in the limestone beds prior to the doming.

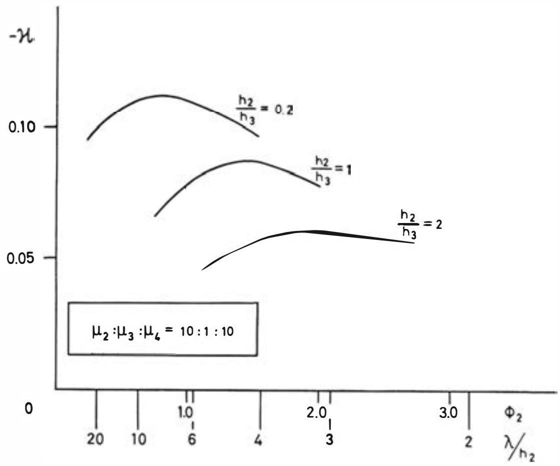

Fig. 7. Kappa-functions for the model shown in Fig. 6. Maxima of the curves give the dominant wavelength-thickness ratios at varying h_2/h_3-ratios and constant viscosity ratios.

To analyse the formation of small domes and ridges, according to the theory of Ramberg, we assume that a layer of limestone mud, h_2 cm thick, with estimated density $\varrho_2 = 2.0$ g/cm^3 and apparent viscosity $\varrho_2 = 1 \cdot 10^{11}$ poises, covers a layer of marl/mud, $h_3 = 10$ cm thick with density $\varrho_3 = 1.8$ g/cm^3 and apparent viscosity $\mu_3 = 1 \cdot 10^{10}$ poises. For substratum we assume an infinitely thick layer of limestone mud whose density is $\varrho_4 = 2.0$ g/cm^3 and viscosity $1 \cdot 10^{11}$ poises. The whole rock complex is then covered by water; cf. Fig. 6. Based on these data the numerical calculations determine the φ_2-values for the dominant wavelengths at different thickness ratios of the marl and limestone layers (Fig. 7). As the thickness of the limestone layer, h_2, decreases the maximum kappa-value occurs for larger wavelength-thickness ratios.

From the exposed section through the Early Arenigian "orthoceratite limestone" at Horns Udde, Lindström (1963, plate 1) and Stephansson (1971b, figs. 19, 20), we notice how the bent limestone layer of the small domes and ridges has a wavelength-thickness ratio which often exceeds 6—10. The theoretical analysis (Fig. 7) indicates that these ratios are only obtained if the thickness of the limestone bed is very small in comparison with that of the marl layer. Hence, to come up with a proper λ/h_2-ratio the viscosity and/or density ratio for the two layers must be changed.

To determine the influence of changing viscosity ratio we study the same type of model with constant thicknesses of the marl and limestone layers while varying viscosity ratio. As the viscosity of the limestone beds is increased the maximum value of $\varkappa$ gives larger values for the dominant wavelength (cf. Fig. 8). These results indicate that a large viscosity contrast between the limestone and the marl prevailed at the time of the doming; and the situation proposed by Wamel seems most probable, namely that "All periods of sedimentation were followed by periods of non-deposition during which lithification started in the newly formed sediment. Obviously this led to the covering of the clay by more or less impermeable limestones, strongly hindering dehydration of the clay material" (Wamel, 1971, p. 299).

Let us assume the viscosity ratios $\mu_2/\mu_3/\mu_4 = 10^4/1/10^4$. Based on these data the numerical calculations according to Ramberg's theory fix the φ_2-value for the dominant wavelength at 0.5 (Fig. 8) which corresponds to $\lambda = 12.6\ h_2$, quite a plausible value for any of the diapirs in the

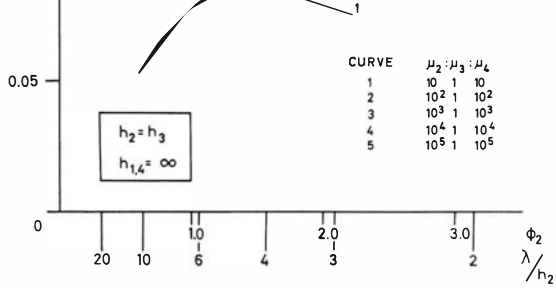

Fig. 8. Kappa-functions for the model shown in Fig. 6. Maxima of the curves give the dominant wavelength-thickness ratios at varying viscosity ratios and constant thicknesses. A large viscosity contrast between marl and limestone gives plausible wavelength values for the small diapirs on Öland.

Early Arenigian beds on Öland. From the computed eigenvector that goes with $\varkappa_1$ we obtain the following proportions between the amplitudes, $y_1/y_2/y_3 = 0.198/1.0/0.0016$. This means that the deflection of the surface of the limestone substratum, y_3, is 0.16 % of the deflection of the top of the marl layer, y_2. A fairly regular bulge of the surface underneath the source layer is also a common feature of the small domes and ridges on Öland, e.g. along the sea cliff at Horns Udde (Stephansson, 1971b).

To determine the rate of amplitude growth and amplification of initial deflections we select $h_2 = h_3 = 10$ cm, $\varrho_2 = 2.0$ g/cm^3, $\varrho_3 = 1.8$ g/cm^3, $\mu_2 = \mu_4 = 1 \cdot 10^{13}$ poises and $\mu_3 = 1 \cdot 10^9$ poises. The calculated values of $q_1 = -0.49 \cdot 10^{-9}$ and $\varkappa = -0.124$ are inserted in eq. (6) to give the ratio getween finite and initial amplitude at various times; cf. Table V. The velocity of amplitudal growth when y_2 is 10 % of the dominant wavelength is $v_2 = \varkappa_1 q_1 y_2 = 0.022$ cm/year.

From numerous observations of small domes and ridges along the western parts of Öland we know that the diapirs started to grow very soon after the deposition of the overburden limestone bed or beds. This is evident from the almost horizontal bedding seen above the bent limestone layer; cf. Lindström (1963, plate I), Stephansson (1971b, fig. 20) and Wamel (1971, fig. 4). Now we find that both the computed amplification of the bent limestone layer (Table V) and velocity of growth for the dominant wave, $v_2 = 0.022$ cm/year, fit the interpretation of Lindström (1963, p. 276) that the average rate of sedimentation should not have exceeded 1 mm/1000 years, in Early Arenigian time in Öland. The computations demonstrate that the bent limestone layer was able to grow and stand upright on the sea-flood during the deposition of the very next layer.

So far we have not taken changes in density into consideration. Assume a four-layer model with a configuration according to Fig. 6 where $h_2/h_3 = 1$ and $\mu_2/\mu_3/\mu_4 = 10/1/10$. A variation of the density ratio ϱ_2/ϱ_3 from 1.11 to 1.45 which could be a variation of limestone density from 2.0 g/cm^3 to 2.6 g/cm^3 at a constant marl density of 1.8 g/cm^3, decreases the φ_2-value from 1.5 to only 1.3. Hence, the effect of increasing the density contrast is to increase the value of the dominant wavelength, but the influence upon the wavelength is of secondary importance in comparison with the effect on the wavelength of the viscosity contrast. From this we are able to conclude that the small domes and ridges of Early Arenigian age on Öland were formed when there was a large contrast in viscosity between the overburden of limestone an dthe source layer of marl. This is a result which lends support to the idea of Jaanusson (1961) who suggested that the limestone underlying a discontinuity surface (the sharply defined surfaces that indicate an interruption in normal sedimentation) was lithified before such a surface attained its final shape.*

Table V. *Amplification of deflection of a small dome or ridge.*

Years	1	10	100	200	1000
y_2/y_{02}	1.019	1.21	6.96	48.42	$2.66 \cdot 10^8$

Formation of diapirs in a multilayered sequence

On the Great Alvar of Öland we find upright, sub-horizontal anticlines of limestone rising above the flat-lying surroundings. Their wavelength is around 10 m and their height sometimes reaches 2 m (Stephansson, 1971b). The term *multilayer anticlinal diapir* is suggested for this type of structure since the emplacement is due to the gravitational instability of several layers of low-density marly and shaly intercalations in the limestone unit. Domes, with diameters of 5 to 15 m, are rather common structures on Öland and sometimes domains with five to ten regularly spaced domes occur. This type of dome has a similar origin to the multilayer anticlinal diapirs .

Very representative of the *multilayer domical diapir* type is a dome in an old quarry 1.5 km NNW of Ö. Vannborga in northern Öland (Stephansson, op. cit., fig. 18). The bottom part of the

* During proof-reading the author's attention has been directed toward the submarine anticlines described by Shinn (1969).

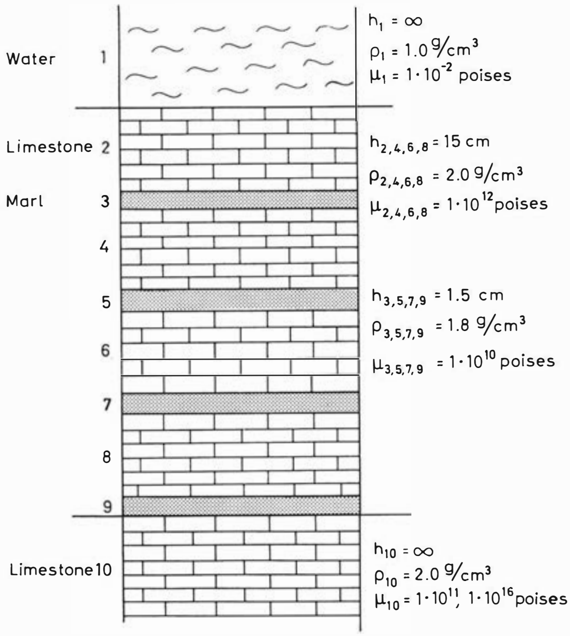

Fig. 9. Model for calculating the dominant wavelength of a multi-layer domical diapir.

dome has a diameter of less than 4 m gradually diminishing upwards. The cessation of growth was followed by horizontal deposition of limestone. The dome at Ö. Vannborga is taken as a pattern for the theoretical analysis of gravitational instability in a multilayer complex.

Assume a model consisting of four layers of limestone of thickness 15 cm, separated by four thin layers of marl or shale of thickness 1.5 cm, resting on a substratum of limestone. The rock complex is covered by water. Assume moreover that the viscosity ratio is 10 and the density ratio is 1.11 between the more competent, denser limestone and the marl (Fig. 9). In this example the maximum value of $-\varkappa$ defines a dominant wavelength fixed by $\varphi_2 = 1.8$, i.e. $\lambda = 3.48\ h_2$ (Fig. 10). From this we may conclude that the buoyant growth of a diapir in a multilayer complex with the dimensions of the structure at Ö. Vannborga and with a small viscosity contrast between the limestone and the marly or shaly intercalations, is unlikely.

By analogy with the analysis of the small domes and ridges, where the layers of limestone seem to have been lithified before sedimentation of the very next layer, we will take the same multilayer model (Fig. 9), but now with a large viscosity contrast, $1\cdot 10^6$, between the limestone and the marls or shales. For a viscosity contrast of 10^6 we obtain a maximum of the kappa-function at $\varphi_2 = 0.4$, i.e. $\lambda = 15.7\ h_2$ (Fig. 10). With an estimated average thickness of 15 cm for the limestone layers, the dominant wavelength is 2.36 m. This is in good agreement with the mean diameter of the dome at Ö. Vannborga and, therefore, there is a good possibility that dome formation occurred when the intercalations were still soft and the limestone beds hardened. From the computed eigenvector associated with the maximum value of $\varkappa$ we derived the following proportions between the amplitudes of the interfaces, $y_1/y_2/y_3/y_4/y_5/y_6/y_7/y_8/y_9 = 0.0189/0.0297/0.641/0.720/0.898/1.0/0.643/0.711/0.023$. This means that the maximum deflection appears on the interface between layer 6 and 7 (cf. Fig. 9) and that the deflection of the top of the rock sequence is 1.89 % of the maximum value.

For $h_2 = 15$ cm, $\varrho_1 - \varrho_2 = -1$ g/cm^3 and $\mu_2 = 10^{16}$ poises, q_1 is $7.35\cdot 10^{-13}$. Insertion of

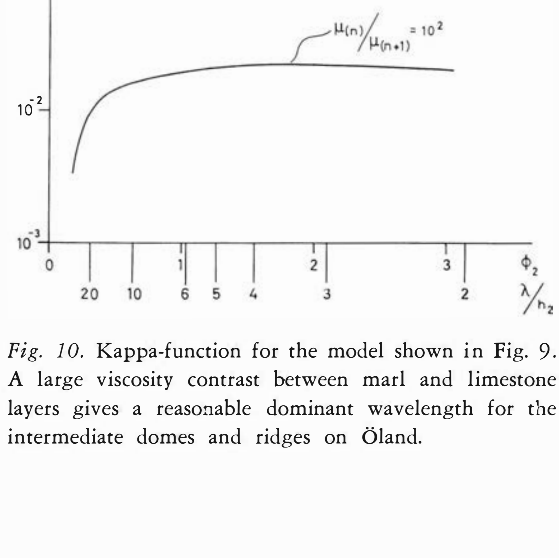

Fig. 10. Kappa-function for the model shown in Fig. 9. A large viscosity contrast between marl and limestone layers gives a reasonable dominant wavelength for the intermediate domes and ridges on Öland.

Table VI. *Amplification of deflection of multi-layer diapirs.*

		Time in years				
$\mu_{2,4,6,8}/\mu_{3,5,7,9}$	Amplification	10^2	10^3	10^4	10^5	10^6
10^6	y_2/y_{02}	1.0022	1.022	1.253	9.583	$6.53 \cdot 10^9$

q_1 and $\varkappa_1$ into eq. (6) gives the ratio between finite and initial amplitudes at various times (Table VI). An amplification of 1.25 in 10^4 years seems most appropriate for the stage of growth reached by the Ö. Vannborga dome considering the estimated rate of sedimentation of 1 mm/1000 years.

As stated earlier, structures having identical corresponding viscosity ratios, thickness ratios and density ratios, subjected to the same field of gravity will remain geometrically similar during their evolution (Ramberg, 1968a). Hence, the results of the theoretical analysis of the multilayer domical diapir at Ö. Vannborga can also be applied to other multilayer diapirs. By assuming a multilayer sequence consisting of layers of limestone one metre thick and intercalations of plastic marl or shale 0.1 m thick and keeping all other parameters unaltered we obtain a dominant wavelength $\lambda =$ 15.7 m. This is an appropriate value for the hump-back ridges and the intermediate domes on the Great Alvar of southern Öland (Stephansson, 1971b).

MODEL EXPERIMENTS STUDIED BY THE CENTRIFUGE TECHNIQUE

The introduction of the centrifuge method by Ramberg (1963) must be regarded as a mile stone in tectonic model experiments. In a series of papers (1963, 1967, 1970) Ramberg has shown that the centrifuge technique is very suitable for model studies of a variety of tectonic phenomena, e.g. formation of batholiths, domes and folds, extrusion of lava, convection currents and continental drift, all powered or strongly influenced by the pull of gravity.

The centripetal acceleration in a centrifuged dynamic model plays the role of gravity in a geologic structure. The increase in acceleration permits the use of model materials that are several thousand times stronger than material used in non-centrifuge models.

A full description of the technique, the centrifuge set-up and the model materials is given in Ramberg (1967). In this study we shall concentrate on application of the method to the initiation of diapirs, calculation of the time needed for evolution of the Mossberga Dome using a scale-model and finally fracturing of brittle model substances in the vicinity of a diapir.

Initiation of diapirs

In a model study of salt-dome tectonics Parker and McDowell (1955) demonstrated the formation of various experimental domes. In their experiments asphalt was used to represent the salt, and weak muds of greater density represented the sedimentary overburden. The models were subjected to the influence of gravity and upward growth of domes was produced by the contrast in the densities of the model materials. The domes were initiated in a series of experiments employing irregularities of the upper asphalt surface, variations of overburden thickness and lateral variations of overburden densities. The theory of dome initiation has been treated thoroughly by Ramberg (1963, 1967, 1970).

Theoretically, a dome can not start growing if both source layer and overburden are uniform and parallel to the equipotential surfaces in a body-force field. However, oil-syrup models affected by gravity and centrifuged models show that diapirism may start in a metastable system with very small irregularities — at molecular level for the liquid models (Ramberg, 1967, p. 95). If the source layer and the overburden possess a finite strength the growth of a diapir will occur only if an irregularity is large enough that the force resulting from the density contrast of overburden

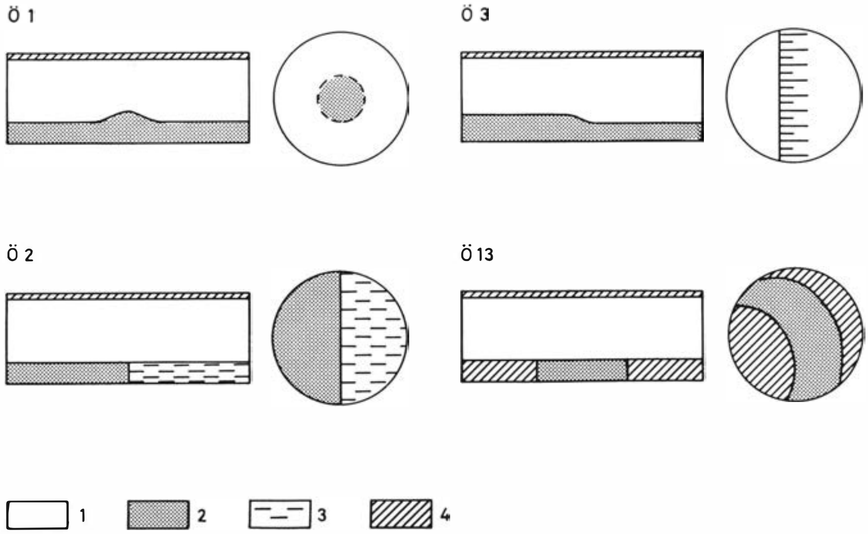

Fig. 11. Initiation of diapirs by irregularities and discontinuities in the source layer. Cross-sections and plans of the models prior to their being run in the centrifuge; model materials: 1, grey painter's putty; 2, silicone putty, $\mu = 6 \cdot 10^5$ poises; 3, soft silicone putty, $\mu = 2 \cdot 10^5$ poises; 4, modelling clay. The density ratio between source layer and overburden is around 0.6.

and source layer is great enough to overcome the 'plunging strength of the overburden'.

Irregularities and discontinuities in the source layer

Perhaps the simplest situation in which a diapir will form is where the overburden rests upon a source layer which has an irregularity in its upper surface. A number of authors, e.g. Dobrin (1941), Nettleton (1943), Parker and McDowell (1955), have suggested salt domes may form in this way.

In a series of models described below the initiation of diapirs originating from irregularities and discontinuities in the source layer has been studied by means of the centrifuge technique (Fig. 11). A description of the model materials used in the experiments is given in Ramberg (1967, p. 84) and a comparison of the mechanical and rheological behaviour of rocks and model materials is presented in Stephansson (1967).

Model Ö1. In a centrifuge cup with a diameter of 200 mm, a 5 mm thick buoyant layer of pure silicone putty was placed on a rigid plate, with surface shaped parallel to the equipotential surface. On top of the layer a 3 mm high "initiating bulge" was placed. A 20 mm thick overburden of painter's putty was placed above the buoyant layer. The surface of the overburden was then covered by a very thin layer of white modelling clay. The overburden of painter's putty had a density of 1.86 g/cm^3 and an apparent viscosity in the range $10^6 - 10^7$ poises, whereas the buoyant layer of silicone putty had a density of 1.12 g/cm^3 and an apparent viscosity of $6 \cdot 10^5$ poises. The model was run in the centrifuge for 45 seconds at an acceleration of 1000 g.

As the diapir reached the surface fractures were formed in the surface sheet. Later, when the diapir started to spread laterally on the surface the thin sheet of modelling clay developed buckling structures in front of the spreading diapir (Fig. 12). A section across the model reveals the typical geometric shape of a dome, including the marginal sink, the root region, the trunk region and the hat of the dome. These typical features of domes are apparent in a great number of centrifuged models figured in Ramberg (1967).

Model Ö3. This model was identical to model Ö1 except that here the irregularity consisted of a sudden change in thickness of the source layer of silicone putty (Fig. 13). After a run of 110 seconds in the centrifuge at 1000 g a ridge penetrated the surface above the edge of the thickness irregularity. Large strong tension cracks appeared in the painter's putty and modelling clay in the ridge centre with buckling on both sides. All along the edge of the thickness variation an asymmetrical sub-surface ridge was formed as shown in the cross-section of the model. The bottommost layer of painter's putty shown in the cross-section was attached to the model after the run in the centrifuge.

Model Ö2. This model was constructed in the same way as those just described but in this case with no irregularity in the interface between the source layer and the overburden. One half of the source layer consisted of soft silicone putty of density 1.13 g/cm^3 and viscosity $2 \cdot 10^5$ poises, and the other half was made of another type of silicone putty with almost the same density but with a much higher viscosity $1 \cdot 10^6$ poises. Diapirs started to grow in the low-viscosity layer and eventually pierced the overburden without any tendency for irregularities to appear on the surface of the stiff layer (Fig. 14). This model was run at 1000 g for 115 seconds.

Model Ö13. In this model the discontinuity in the source layer in plan consisted of a slightly curved layer of silicone putty, $\varrho = 1.2$ g/cm^3, surrounded on both sides by layers of stiff modelling clay, $\varrho = 1.68$ g/cm^3. The overburden consisted of painter's putty, $\varrho = 1.86$ g/cm^3. Without any initial thickness irregularities a curved ridge was formed which split into separate domes in the

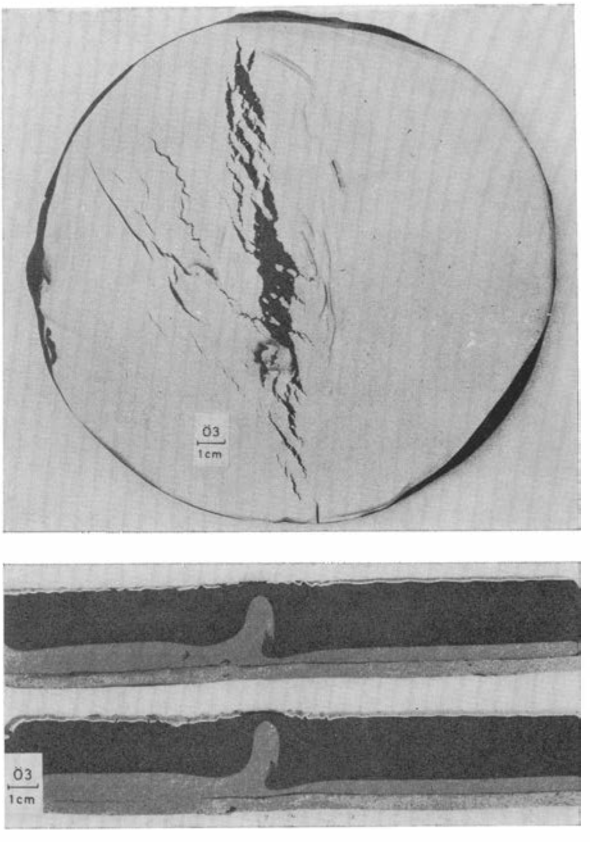

Fig. 13. Surface and cross-section of model Ö3. A ridge was formed at the edge of the thickness irregularity in the source layer. The bottommost layer of painter's putty in this model and others of this series was attached to the model after the run in the centrifuge to prevent flowing. Run 110 sec. at 1000 g.

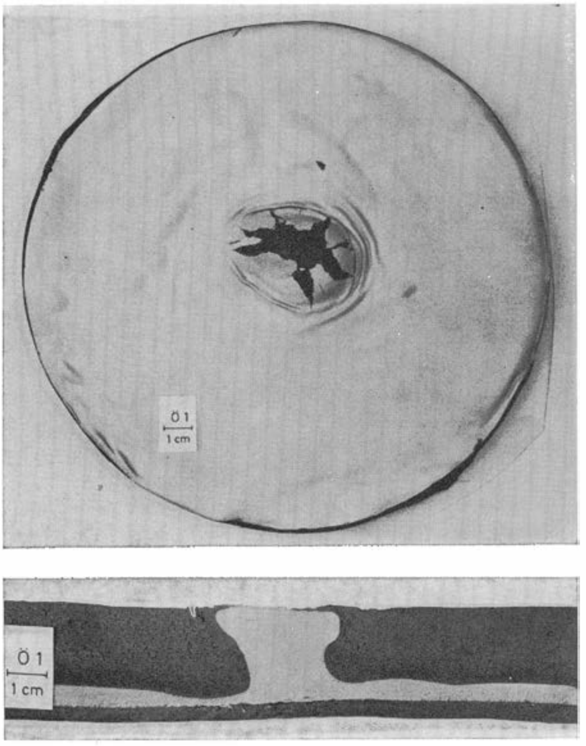

Fig. 12. Surface and cross-section of model Ö1, showing intense stretching and buckling of the thin top layer of modelling clay and the typical shape of a dome with a well-developed marginal sink. The dome was initiated by a bulge on the surface of the source layer. Run 45 sec. at 1000 g.

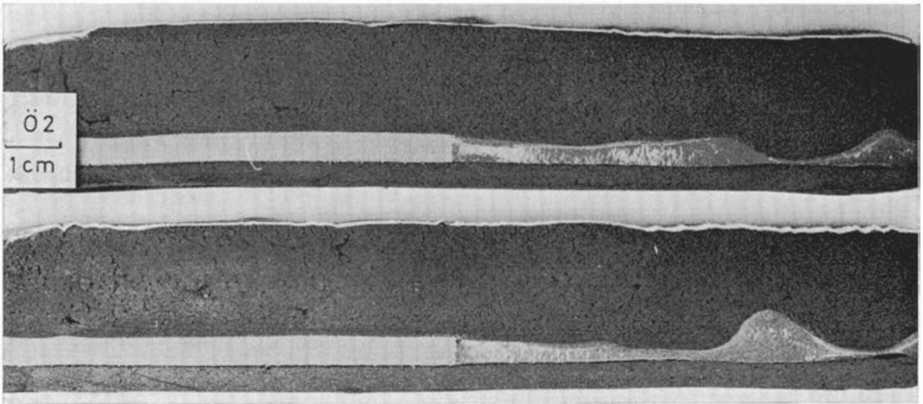

Fig. 14. Cross-sections of model Ö2 after being run in the centrifuge for 115 sec. at 1000 g. The viscosity discontinuity in the source layer gives a gravitational instability first in the soft layer of silicone putty.

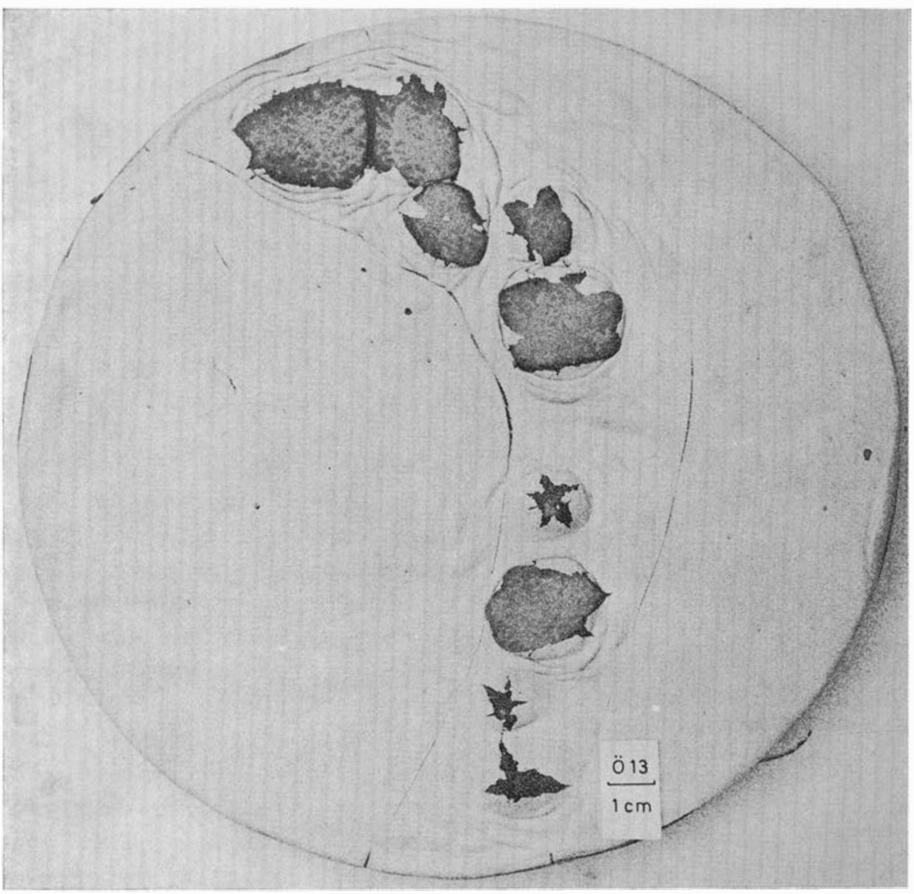

Fig. 15. Model Ö13 as seen from above after being run for 120 sec. at 2000 g. The domes have penetrated the overburden in the centre of the curved source layer. The borders of the source layer are indicated on the surface.

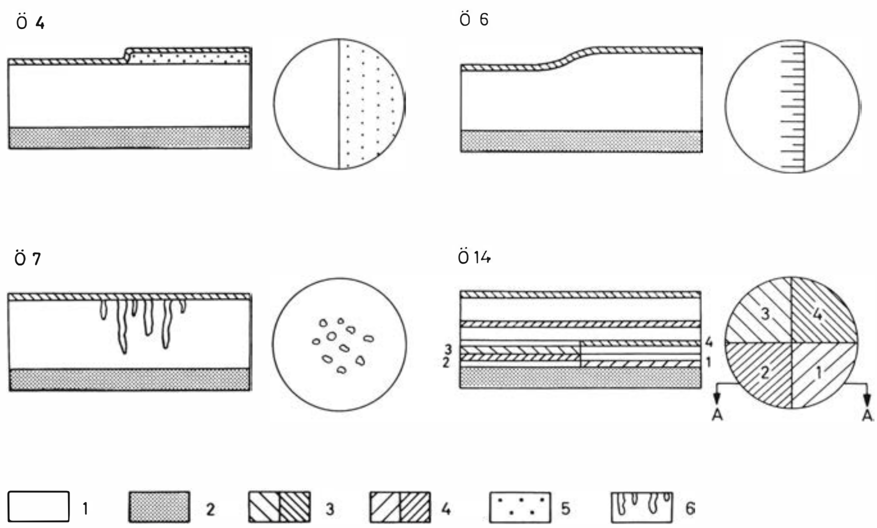

Fig. 16. Initiation of diapirs by irregularities and discontinuities in the overburden. Cross-sections and plans of the models prior to their being run in the centrifuge. Model materials: 1, grey painter's putty; 2, silicone putty; 3, 4, modelling clay; 5, stiff painter's putty; 6, holes.

final stage of the experiment run for 120 seconds at 2000 g. The border of the buoyant layer is apparent on the photograph of the top surface of the model (Fig. 15).

From model experiments employing a buoyant sheet of silicone putty below an overburden of syrup we know that the localization of diapiric growth is strictly controlled by the shape of the buoyant layer; cf. Ramberg (1967, figs. 12, 13). Hence, a source layer with a curved outer boundary favours the development of curved anticlinal ridges which may later be split up into separate domes. Such a curved outer boundary may well have controlled the final shape of the curved single-layer anticlinal diapir found on northern Öland (Stephansson, 1971b, figs. 21, 22).

Irregularities and discontinuities in the overburden

Any area of decreased thickness of overburden is an area of decreased pressure on the source layer, where a diapir may be initiated. This method of initiation was used by Nettleton and Elkins (1947), Parker and McDowell (1955) and Ramberg (1963, 1967) in their model experiments of dome initiation.

Model Ö4. In this experiment the source material was a 5 mm thick layer of silicone putty of viscosity

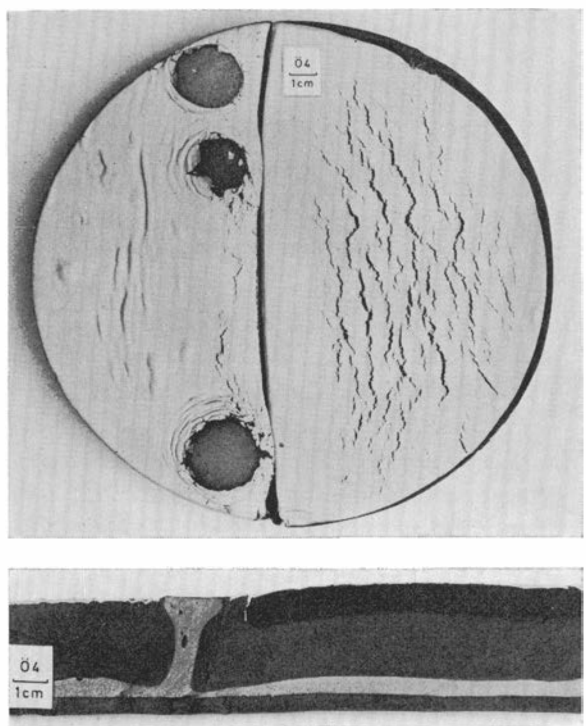

Fig. 17. Surface and cross-section of model Ö4. The excess overburden of painter's putty favours diapirism along the edge of the discontinuity. The flow of excess overburden material towards the edge causes tension cracks on the surface. Run 8 min. at 1000 g and 3 min. at 3000 g.

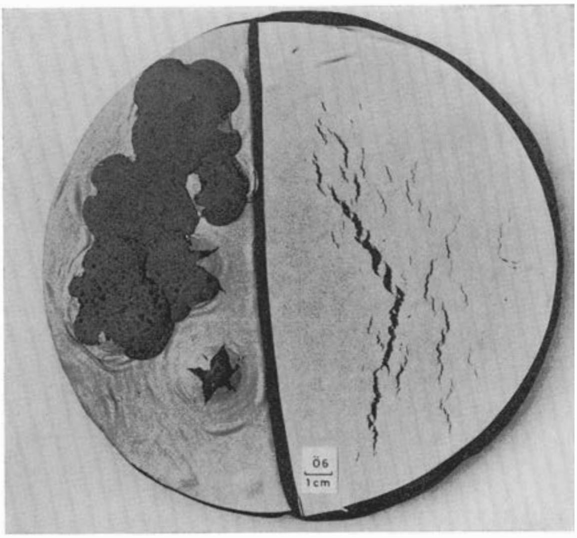

Fig. 18. Surface of model Ö6. A gradual change in overburden thickness causes a more distributed appearance of domes in the area of least thickness. Run 10 min. at 1000 g.

$6 \cdot 10^5$ poises, having a plane interface with the overburden which was a layer of painter's putty 20 mm thick covered by a thin layer of modelling clay. In model Ö4 half the top surface was covered by a 1 m thick layer of stiff painter's putty (Fig. 16).

After 8 minutes' run at 1000 g and 3 minutes' at 2000 g a ridge formed just on the side of the edge discontinuity, and this ridge later split up into separate domes. The plastic behaviour of the excess overburden caused a flow of this material towards the edge and tension cracks formed perpendicular to the direction of flow, replacing each other in en echelon pattern (Fig. 17). According to Ramberg (1963, p. 30) the tendency for domes to form along discontinuities in overburden load is related to the rather abrupt increase of horizontal pressure gradient across such discontinuities. This creates a pressure difference in the source layer on either side of the edge resulting in horizontal flow in this layer. As a consequence a local bulge develops in the source layer just away from the edge of excess overburden (Fig. 17).

Model Ö6. It is not necessary that the change of overburden thickness be abrupt. A gradual change in thickness also generates a pressure gradient which leads to lateral flow along the source layer (Ramberg, 1967, p. 99). This situation is illustrated in model Ö6, where the top surface of the overburden has a gentle slope. Compared to the situation in model Ö4 the diapirs protruded into the thin parts of the overburden more randomly (Fig. 18). The model was run for slightly less than 10 minutes at an acceleration corresponding to 1000 g.

This type of initiation — a gradual change in overburden thickness — may have been of importance in the formation of small domes and ridges in the Early Arenigian limestone beds on the island of Öland. This part of the limestone succession, especially the rocks of the Billingen Stage, contain irregularly layered marly limestone and massive limestone beds; cf. the section at Horns Udde (Lindström, 1963, plate 1).

Model Ö7. Many of the Ordovician limestone beds on Öland have a surface morphology that includes small or large irregularities in the form of branching tubules from boring organisms and 'corrosion pits' due to chemical solution. These structures are intimately related to the so-called discontinuity surface (see p. 179). As already mentioned many discontinuity surfaces according to Jaanusson (1961) and Lindström (op. cit.) show clear evidence of having been lithified prior to the deposition of the overlying beds. As the theoretical calculations (p. 177) indicate that the growth of small domes and anticlines took place when there was a large viscosity contrast between the limestone layer and the underlying marl, a situation requiring a lithified limestone bed to cover a plastic marl, the tubules and corrosion pits may well have been of importance for the dome initiation. A concentration or local deepening of tubules or pits decreases the bending resistance or lowers the moment of inertia of the limestone bed and, hence, favours the growth of a ridge or a dome.

In the middle of the overburden of painter's putty in this model borings were made, some reaching almost to the overburden — source-layer interface. After 6 minutes' run at 2000 g the model was sliced. The silicone putty had formed a dome situated in the centre of the model where the borings were deepest (Fig. 19).

Model Ö14. This model consisted of the following sequence of layers started from the bottom: a 5 mm thick layer of silicone putty, a 2 mm thick layer of painter's putty of which a sector of $\pi/2$ was replaced by a white modelling clay, another three layers of painter's putty each one 2 mm thick containing a sector of modelling clay rotated 90° clockwise with respect to the layer below (cf. Fig. 16), a 10 mm thick layer of painter's putty, a thin, 0.2 mm, layer of modelling clay, a further 10 mm of painter's putty and finally, a thin cover of white modelling clay on top of the model.

After 160 seconds' run in the centrifuge at 2000 g four domes had penetrated the overburden of that half of the model which contained layers 3 and 4 in the sketch of the initial arrangement (Fig. 16). Cross-sections for half the model parallel to the section A-A show only a slight bulging of the layer of modelling clay (1) situated in contact with the source layer. The left hand ends of the sections show how the source layer is able to form

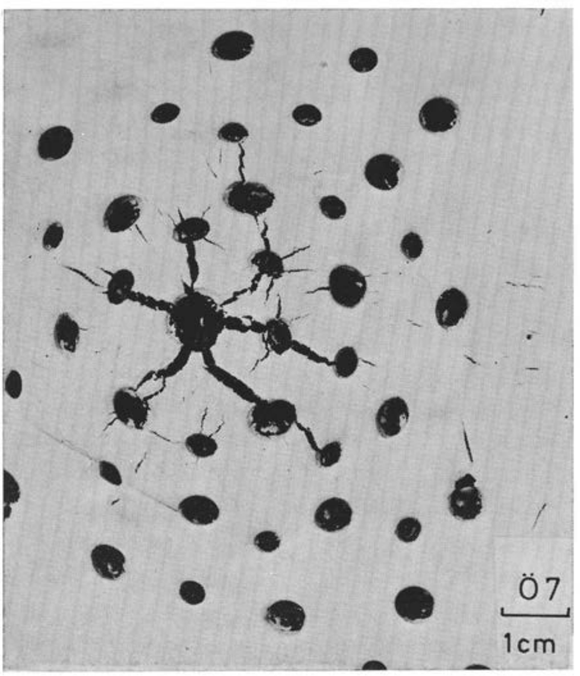

Fig. 19. Part of the surface of model Ö7. A dome was formed in the model in the region of deepest borings in the overburden. Run 6 min. at 2000 g.

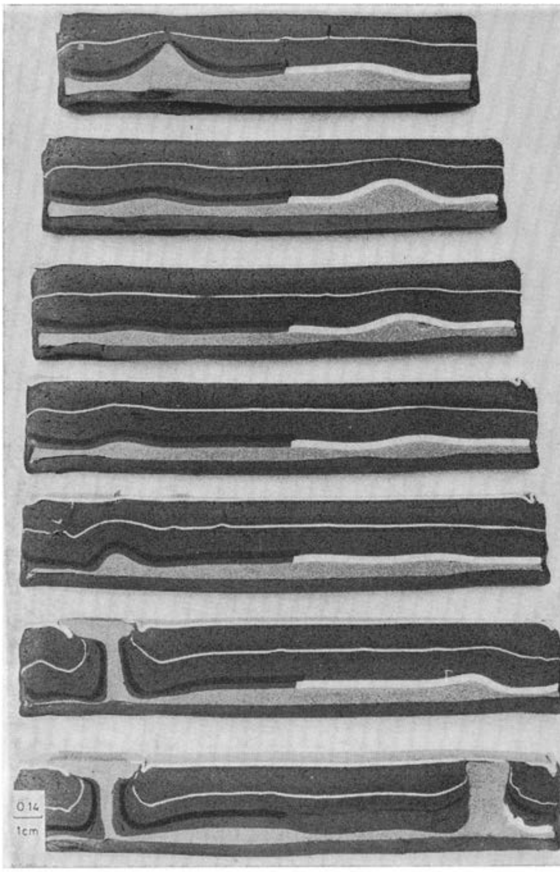

Fig. 20. Cross-sections of model Ö14. In places where the source layer is overlain by a stiff layer of modelling clay only a slight bulging appears, to the right in the sections. A layer of painter's putty between the source layer and modelling clay facilitates doming. Run 160 sec. at 2000 g.

larger bulges (Fig. 20). This is due to the fact that diapirs can be initiated more easily at a soft source layer — overburden interface, here represented by the 2 mm thick layer of painter's putty. Towards the middle of the model, in the boundary region between layers 2—3 and 1—4 respectively, the silicone putty has protruded into the overburden because the concentration of discontinuities is most frequent in this region of the model.

A close examination of the model in the section A-A shows two types of structures often met with in the Early Arenigian limestones of Öland. The diapir to the left in the upper cross-section of Fig. 21 has a peaked top and the more compe-

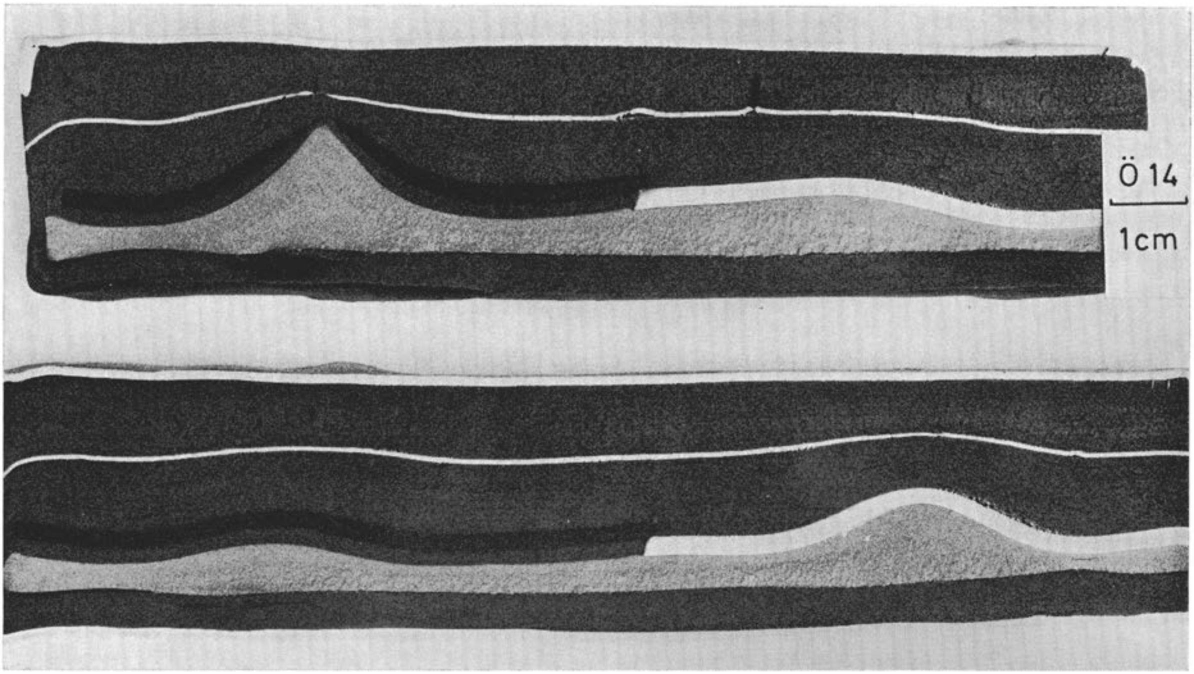

Fig. 21. Details of model Ö14. Note the strong thinning in both flanks of the diapir in the left part of the upper section. The structures show striking similarities to the small diapirs on Öland; cf. Stephansson 1971b, figs. 20, 22.

tent layer of modelling clay has been broken and shows strong thinning on both flanks; cf. Stephansson (1971b, figs. 20, 22). The diapir to the right in the lower section shows a gentle bulging of the competent layer of modelling clay. This structure is typical of the small diapirs on Öland. It is worth noting the bending of the thin layer of modelling clay in the overburden in these sections, a situation seldom met with on Öland because the doming ceased before deposition of the next layer.

Irregularities and discontinuities in the substratum

Model Ö12. In the study of peripheral-sink development in dome models of asphalt and mud Parker and McDowell (1955) studied a model with a configuration very similar to that of model Ö12. The salt structure in NW Germany and adjoining parts of the North Sea are strictly controlled by the form of the Zechstein basin and a schematic model similar to Ö12 has been used by Trusheim (1960) to illustrate the relationship between the thickness of the salt and the diapiric structures. Salt walls in the centre of the basin succeeded outward by salt stocks and finally salt pillows along the border of the basin is the most common distribution.

The model for illustrating the initiation of diapirs, where the substratum has a certain slope and forms a basin, is shown in Fig. 22. No irregularities were made in the source layer — overburden interface. The model was run at an acceleration of 2000 g for 45 seconds. A huge single dome and twin-domes were formed at each end of the valley. A section through the twin domes shows their strong relief or height above the surface of the overburden (Fig. 23). It is also apparent that their trunk axes are perpendicular to the surfaces of the slopes.

Model Ö16. A bulge with a diameter of 6 cm and a height of 5 mm was placed as a substratum irregularity in the centre of the model. After 80 seconds' run at 2000 g joints on the surface of the overburden indicated a diapir below. A cross-

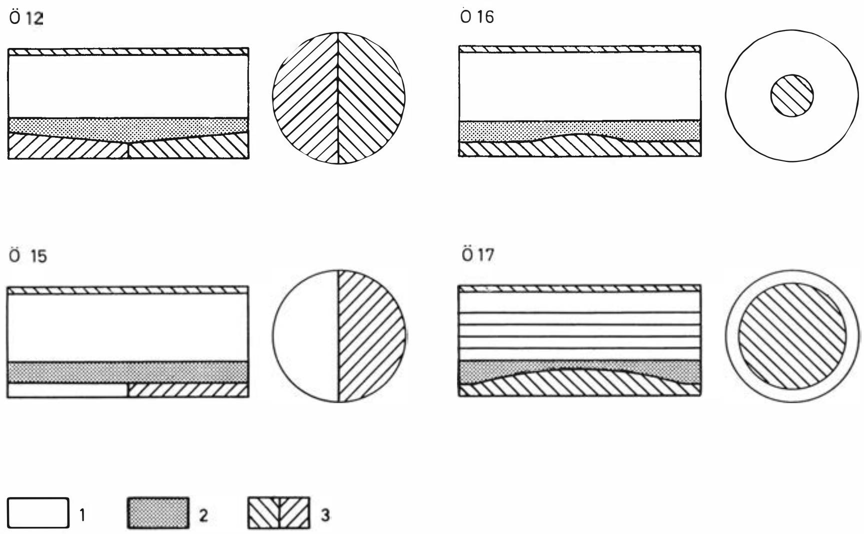

Fig. 22. Initiation of diapirs by irregularities and discontinuities in the substratum. Cross-sections and plans prior to centrifuging. Model materials: 1, painter's putty; 2, silicone putty; 3, modelling clay.

section of the fairly symmetrical dome is shown in Fig. 24.

Model Ö17. As in model Ö16 the irregularity here consisted of a bulge in the substratum below the source layer but now with a diameter of about 15 cm. The source layer consisted of two layers of silicone putty with a total thickness of 6 mm. The overburden of painter's putty contained four thin layers of modelling clay in its lower and central part and a thin layer was placed on the surface of the model. The model was run for 80 seconds at 2000 g. After slicing it was noticed that the buoyant layer of silicone putty had ascended through the overburden along the edge of the model (Fig. 25). Although a pressure difference in the source layer existed along the whole surface of the initial bulge the dome-generating effect dominated at the base of the bulge where the source layer had its greatest thickness.

Model Ö15. A discontinuity in the basement was produced by constructing a layer of painter's putty and modelling clay, each forming one half of the model. After 90 seconds' run in the centrifuge at 2000 g the model was sectioned and it was noticed that the diapirs had started to grow above the layer of soft painter's putty (Fig. 26). As the substratum below the source layer is non-rigid it

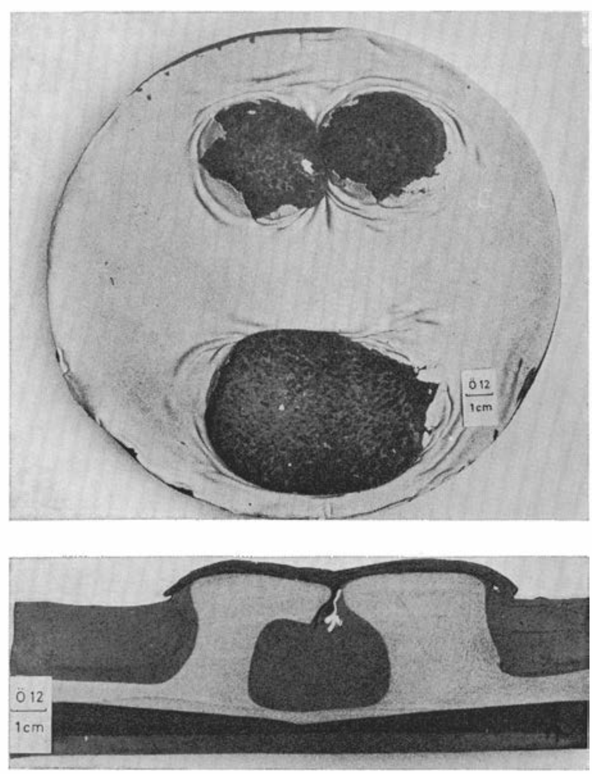

Fig. 23. Surface and cross-section of model Ö12. The domes are concentrated in areas with the largest thickness of source layer .Section of twin-domes showing trunk axes perpendicular to the surface of the substratum. Run 45 sec. at 2000 g.

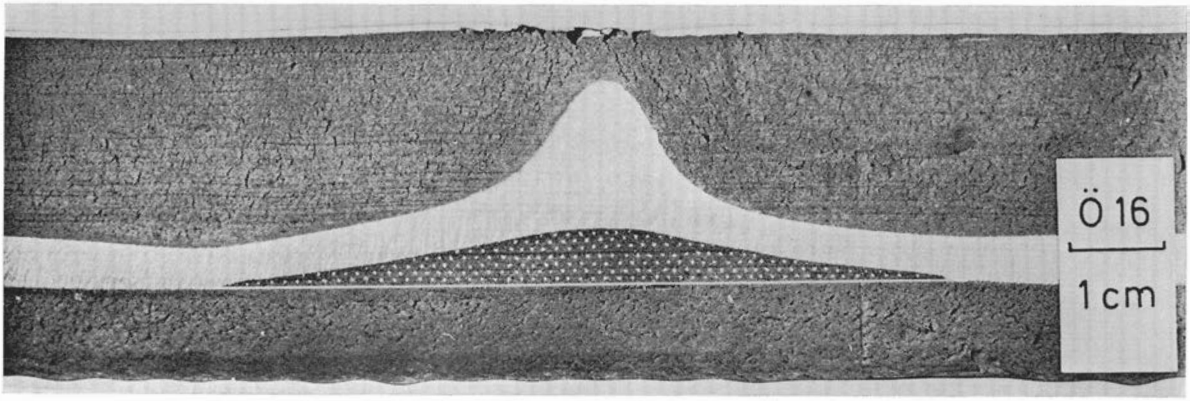

Fig. 24. Cross-section through the centre of model Ö16. A bulge in the substratum caused the doming. Run 80 sec. at 2000 g.

tends to participate in the formation of the dome by forming a bulge directly below the trunk. The active participation of the substratum is a common phenomenon in centrifuged models; cf. Ramberg (1967, figs. 62, 63), and is in accordance with the theory of garvity instability.

A slight bulging of the limestone bed situated below a buoyant layer of marl is a feature often met which in diapiric structures in the Early Arenigian limestone on Öland (Stephansson, 1971b). The statement made by the author that the underlying bed of limestone was plastic but nevertheless stiffer than the light buoyant layer during the

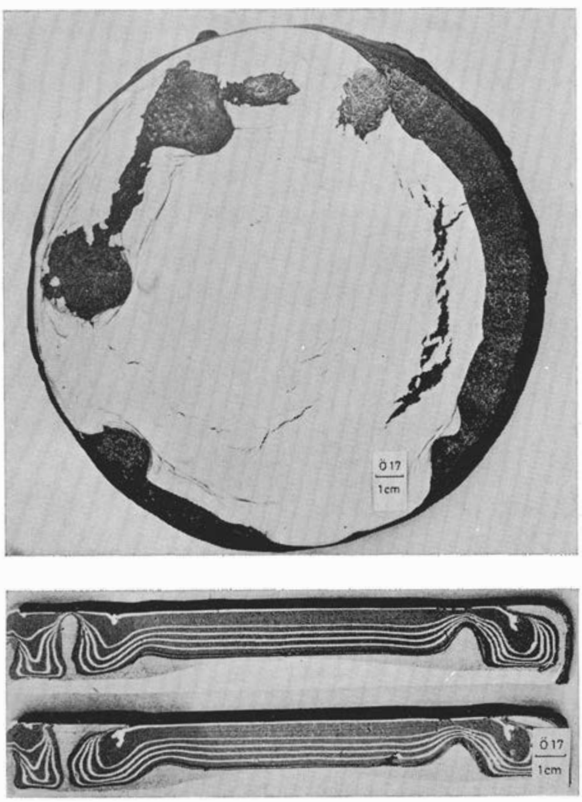

Fig. 25. Surface and sections of model Ö17. The large diameter of the bulge in the substratum led to anticlinal growth around the edge of the model. Run 80 sec. at 2000 g.

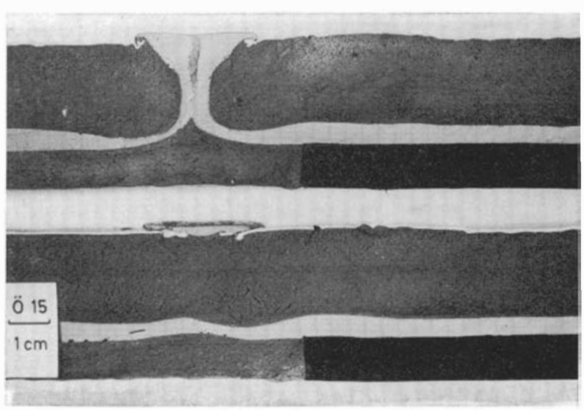

Fig. 26. Cross-sections of model Ö15. The diapir started to grow above the layer of soft painter's putty. Notice the upward drawing of the substratum below the trunk of the dome. Run 90 sec. at 2000 g.

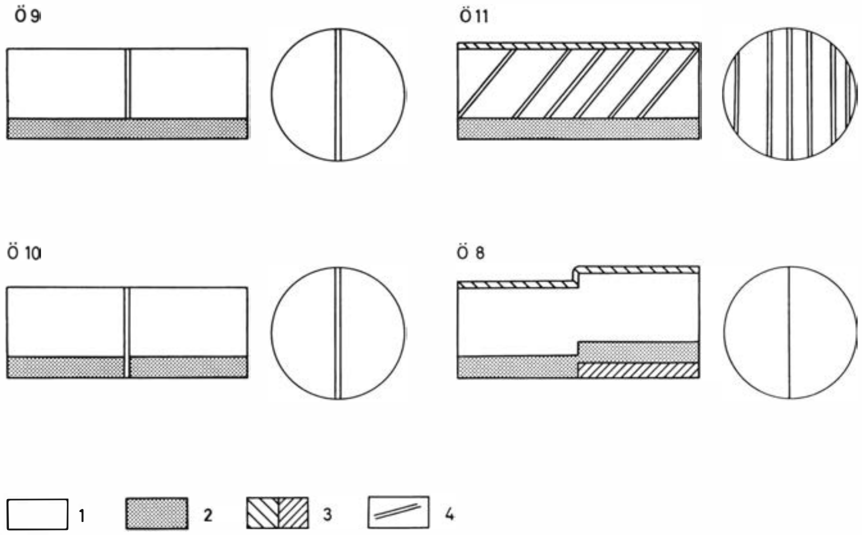

Fig. 27. Initiation of diapirs by jointing and faulting. The joints or faults were simulated by a thin layer of modelling clay, lubricated on both surfaces. Cross-sections and plans prior to centrifuging. Model materials: 1, painter's putty; 2, silicone putty; 3, modelling clay; 4, simulated joint or fault.

gravitational doming is valid because the theoretical results demonstrate that both the overburden and substratum of limestone were much more viscous than the buoyant layer of marl at the time of diapiric growth (Stephansson, op. cit., p. 73).

The influence of jointing and faulting on the initiation of diapirs

As far as the writer knows the influence of jointing and faulting on the initiation of diapirs has not been studied experimentally until now. Parker and McDowell (1955) discuss the possible consequences of a fault which cuts a source layer. The asphalt they used as a source layer in their experiments could not separate along a plane surface, and they did not succeed in making proper faults. When running models in a centrifuge we can use stiffer materials which maintain the proper shape during model preparation but which are also able to fail under the influence of the centrifugal force field.

In three models of this series of experiments a fault or joint was simulated by a 0.5 mm thick layer of modelling clay. The surfaces of the layer were smeared with a thin film of oil. All models in this series were built up using a 5 mm thick source layer of silicone putty overlain by a 20 mm thick layer of painter's putty.

Model Ö9. The model initially consisted of a simulated joint or fault dividing the overburden into two halves (Fig. 27). After 4 minutes' run at 1000 g followed by 1 minutes' run at 2000 g the silicone putty had penetrated the overburden and formed a row of elongate domes parallel to the joint or fault (Fig. 28). After slicing the model it appeared that the buoyant layer had pushed the layer of modelling clay in front of the rising diapir towards the surface. The initial zone of weakness favoured the emplacement of diapirs with rather narrow trunks.

Model Ö10. In this model the similated joint or fault run right through the model from the bottom of the source layer to the top of the overburden. As in the case of model Ö9 the diapirs were initiated in the source layer at the contact with the layer of modelling clay (Fig. 29). Model Ö10 was run for 140 seconds at 2000 g.

Model Ö11. Six points or faults were arranged to be parallel with a dip of 30° in the centre of the model. After 80 seconds' run at 1000 g a row of separate domes had penetrated the surface in

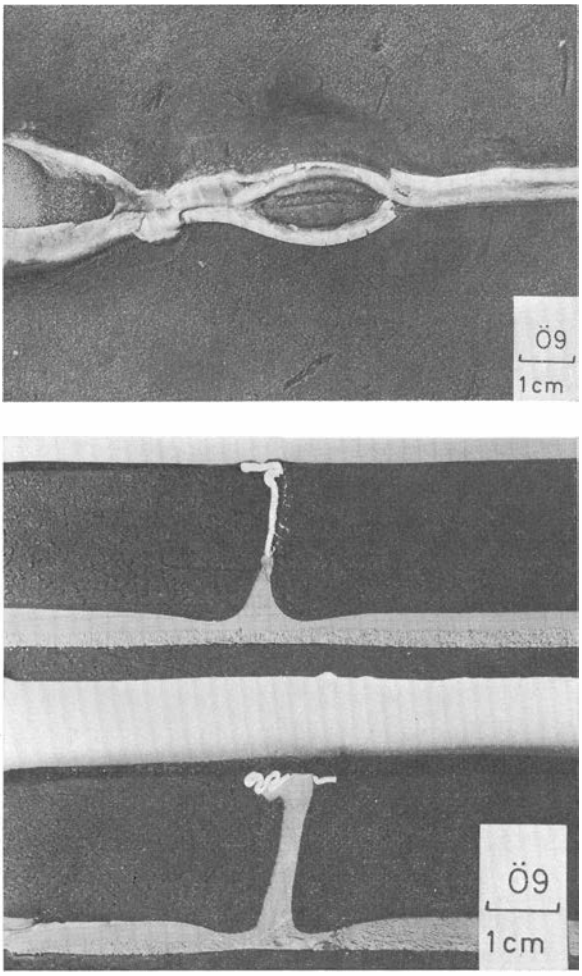

Fig. 28. Detail of the surface and cross-sections of model Ö9. The diapir penetrated the overburden at the weak zone and formed a row of elongate domes on the surface. Notice the rather narrow trunk of the dome. Run 4 min. at 1000 g and 1 min. at 2000 g.

lines almost parallel to the strike of the simulated joints/faults. Slicing of the model clearly demonstrated that the diapirs initiated were in places where the joint or fault comes into contact with the source layer (Fig. 30). Although the initiation was strictly controlled by this contact the piercing movement of the diapir took place in a direction perpendicular to the bottom of the source layer. A much stronger overburden might have forced the diapirs to follow the fault plane on their way up to the surface.

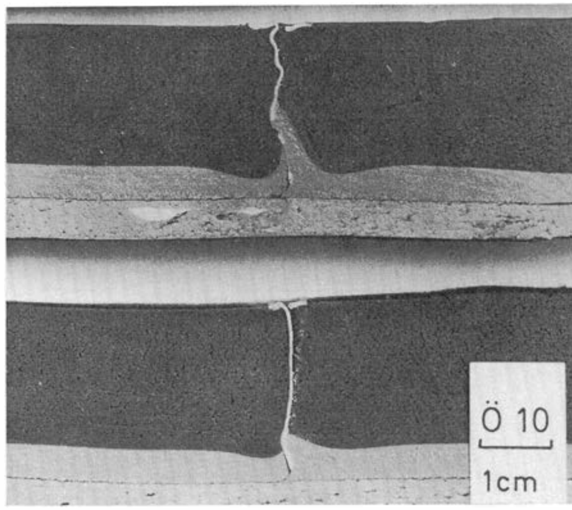

Fig. 29. Sections through model Ö10 after 140 seconds' run at 2000 g. A joint or fault cutting both the overburden and source layer causes dome initiation.

Model Ö8. The last model in this series illustrates the initiation of diapirs at a dip-slip fault, where there is a relative displacement down dip in the fault plane (Fig. 31). After 70 seconds' run at 2000 g material from the source layer had pierced the surface of the model along the edge of the fault and lateral spreading caused an intensive folding of the stiff surface layer of modelling clay. A cross-section of the model showed that the initiation of the diapir had been at the edge of the fault.

The initiation of diapirs due to the presence of faults and joints has been of great importance for many of the structures on the island of Öland, e.g. the main ridges on the southern part seem to have been controlled by weak zones (Stephansson, 1971b, p. 49). Also several of the single-layer anticlinal diapirs from the Billingen Stage in the Lower Ordovician have a pronounced joint running parallel with the hinge line.

Model of the Mossberga Dome

A geologic map and section of the Mossberga Dome on central Öland were figured in an earlier publication of the author (Stephansson, 1971b). This type of dome having a diameter on the scale of kilometers, is not found elsewhere in Öland,

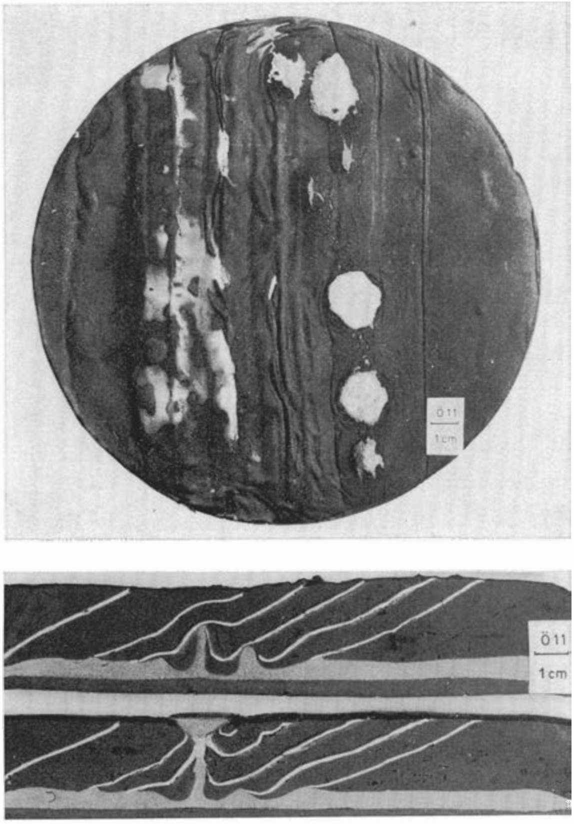

Fig. 30. Surface and cross-sections of model Ö11. The domes on the surface are arranged parallel with the strike of the simulated joints or faults. Diapir initiation takes place where the joints/faults are in contact with the source layer. Run 80 sec. at 1000 g.

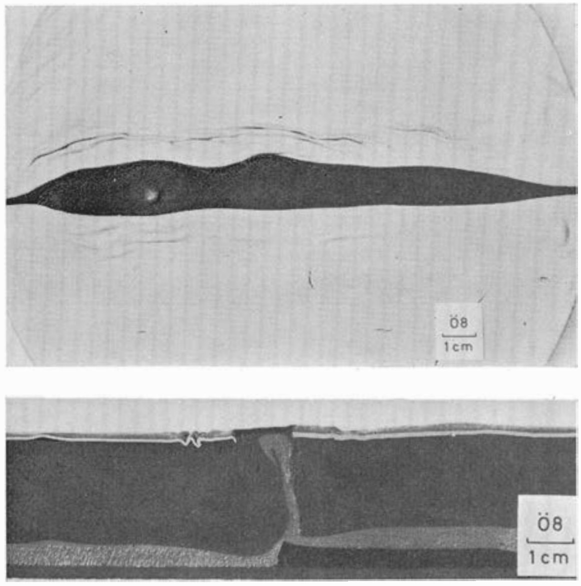

Fig. 31. Detail of the surface and cross-section of model Ö8. A ridge was formed striking along the edge of the fault. Run 70 sec. at 2000 g.

and hence there must have been certain unique factors prevailing at Mossberga which lead to the formation of a dome there. According to Stephansson (op. cit.) the dome-generating irregularity was a quartzite monadnock projecting up into the buoyant layer, a situation which can be fairly well illustrated by means of the source layer — Middle Cambrian shales in the case of the Mossberga Dome — away from the centre of a dome generates a pressure gradient and lateral flow can take place along the thickness gradient. Such a thickness and pressure gradient were developed at Mossberga if the assumption is correct that deposition of the overburden (Ordovician limestones) took place horizontally.

To study the initiation and dynamics of growth of the Mossberga Dome a few scale-models were made. An example of the calculation of the time of evolution of the dome scale-model technique is shown in Table VII. The model (Fig. 32) was scaled geometrically from the geologic map and section presented in Stephansson (1971b, fig. 17). The model ratio of dimension, l_r, was taken using the thickness values. There are no available density measurements or rocks from the Mossberga Dome, so the values given in Table VII were estimated, partly guided by the values given for the borehole at Segerstad, cf. Table I. The density of the heavy painter's putty determined the ratio of density in the model. This ratio, 0.67, was then obtained for the buoyant layers by adding baryte or magnetite powder to the pure silicone putties.

Because the rheological properties of rocks in their natural environment are almost unknown, estimating viscosities is somewhat hazardous. Rather than attempting this the values of viscosity given for the different rock units in the dome itself were taken as the product of the viscosity values of the model materials times a model ratio of 10^{11}. However, the relative values for rocks

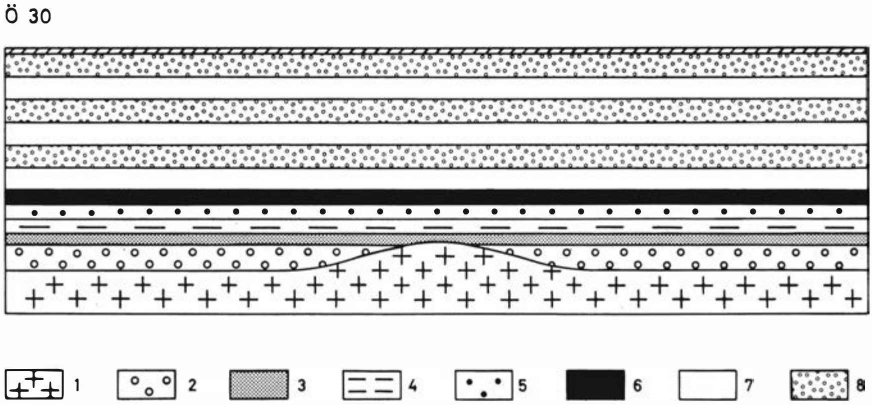

Fig. 32. Section through a scale-model of the Mossberga Dome prior to its being run in the centrifuge. Model materials: 1, modelling clay; 2, white painter's putty; 3, 4, 5, silicone-baryte putty with different densities; 6, silicone-magnetite putty; 7, grey painter's putty; 8, white painter's putty. Thicknesses, densities and viscosities of the different layers are given in Table VII.

in the various stratigraphic units of the sequence are considered to be fairly adequate, for instance the quartzite is assumed to be ten times more viscous that a sandstone and one thousand times more viscous than a soft shale. The rock viscosity values given in Table VII are also in broad agreement with values found from different laboratory investigations (Table III).

The painter's putty employed as an overburden in the model is a material with thixotropic properties. It also possesses the so-called back-lash effect, i.e. the material is at first very soft for an initial small amount of strain and after that it hardens and exhibits a yield point. This non-linear behaviour causes the viscosity to vary between $5 \cdot 10^5 - 5 \cdot 10^7$ poises.

Table VII. *Scale-modul calculation of time needed for the evolution of the Mossberga Dome.*

MATERIAL		THICKNESS			DENSITY			VISCOSITY		
Mossberga Dome	Model Ö 30	M m	Ö 30 mm	Ratio l_r	M g/cm^3	Ö 30 g/cm^3	Ratio ρ_r	M poises	Ö 30 poises	Ratio μ_r
Quarzite	Modelling clay	?	7.5	—	2.5	1.67	0.67	$5 \cdot 10^{19}$	$5 \cdot 10^8$	10^{-11}
Sandstone	White putty	0-80	2.5	—	2.7	1.82	0.67	$5 \cdot 10^{18}$	$5 \cdot 10^7$	10^{-11}
Bituminous shale	Silicone-Baryte putty	12.5	2.5	$2 \cdot 10^{-4}$	2.45	1.64	0.67	$4.9 \cdot 10^{16}$	$4.9 \cdot 10^5$	10^{-11}
Arenaceous shale	Silicone-Baryte putty	14.0	2.8	$2 \cdot 10^{-4}$	2.4	1.60	0.67	$2.1 \cdot 10^{17}$	$2.1 \cdot 10^6$	10^{-11}
Soft shale	Silicone-Baryte putty	12.5	2.5	$2 \cdot 10^{-4}$	2.3	1.54	0.67	$5.0 \cdot 10^{16}$	$5 \cdot 10^5$	10^{-11}
Alum shale Glauconitic shale	Silicone-Magnetite putty	~12.5	2.5	~ $2 \cdot 10^{-4}$	2.2	1.48	0.67	$4.1 \cdot 10^{16}$	$4.1 \cdot 10^5$	10^{-11}
Limestone	White and grey painter's putty	100	20	$2 \cdot 10^{-4}$	2.7	1.82	0.67	$5 \cdot 10^{18}$	$5 \cdot 10^5 - 5 \cdot 10^7$	$10^{-13} - 10^{-11}$

Mossberga Dome	Model Ö 30	
1 g	2000 g	Body force per unit mass
t_o	$t_m = 160$ sec	Time of evolution

$$\sigma_r = \rho_r \cdot l_r a_r = 0.67 \cdot 2 \cdot 10^{-4} \cdot 2000 = 0.27$$

$$t_r = \mu_r \cdot \sigma_r^{-1} = 3.7 \cdot 10^{-11}$$

$$t_o = \frac{t_m}{t_r} = \frac{160}{3.7 \cdot 10^{-11}} = 4.3 \cdot 10^{12} \text{ sec} \sim 0.5 \cdot 10^6 \text{ years}$$

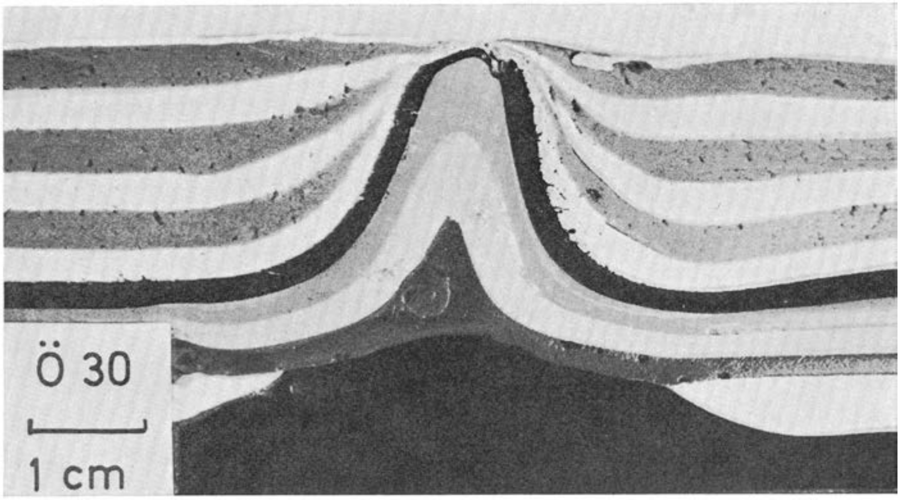

Fig. 33. Cross-sections through the central part of the scale-model of the Mossberga Dome. The doming was initiated above the bulge in the substratum corresponding to the monadnock of quartzite at Mossberga.

After 160 seconds' run at a mean acceleration of 2000 g the topmost stratum of the source layer had penetrated the overburden and was visible on the surface. Cross-sections of the central part of the model showed that diapirism had been initiated at the bulge in the very competent substratum (Fig. 33). In order to know that a diapir formed in a model it must reach the surface of the overburden. Hence, the model has too large amplitude compared with the Mossberga Dome, where the closure is of the order of 30 m. We notice how the movement of the diapir has stretched and bent the layered overburden of painter's putty. The thickening of the individual source layers in the lower part of the trunk zone is due to the position of the cross-sections at the outwardly flank of the dipping trunk.

By applying the scale-model theory presented in Ramberg (1963, 1967) the total time needed for the dome to evolve, is found to be around 1 million years (Table VII). This seems too short a time fo rthe formation of the Mossberga Dome. The calculations for arriving at this value were based on a model ratio of viscosity $\mu_r = 10^{-11}$. For the painter's putty in the overburden this implies a viscosity value $\mu_m = 5 \cdot 10^7$ poises which corresponds to a state of hardened or strained putty. In the initial stage of evolution the value $\mu_m = 5 \cdot 10^5$ poises is more likely. Hence, for the overburden the model ratio would more realistically be $\mu_r = 10^{-13}$. Making use of this value in the equations for determining the time of evolution of the structure gives a value of 50 million years. This is a more realistic time of evolution of the dome but we no longer have a true scale model of the diapiric growth.

Models with brittle fracturing

So far we have been studying models where diapiric deformation by plastic flow has been the main interest. Fracturing has been produced only in models with a thin layer of modelling clay on top of the overburden.

In studying the different diapiric structures on Öland we notice that many of the intermediate and large diapirs are characterised by a high joint frequency, indicating brittle or semi-brittle behaviour of the rock material (Stephansson, 1971b, fig. 12). Brittle fracturing has also been of importance in many of the small structures, especially in the stage of initiation, although a plastic deformation dominates (Stephansson, op. cit., figs. 20, 21).

In a series of model experiments diapirs of stitching wax were allowed to penetrate overburdens of painter's putty with brittle plates em-

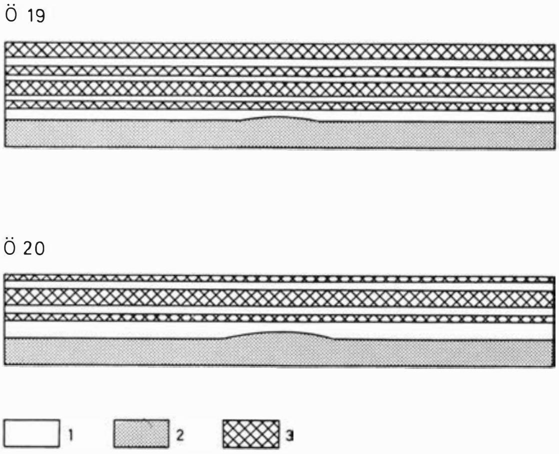

Fig. 34. Cross-sections of models Ö19 and Ö20 prior to their being run in the centrifuge. Model materials: 1, painter's putty; 2, stitching wax; 3, brittle plates of a mixture of sand, plaster and water.

bedded or multilayers of putty and plates. The wax was produced from a mixture of collophony and ethylene phthalate having a density of 1.2 g/cm^3 and a viscosity of $5 \cdot 10^7$ poises. This material has been used in several of Ramberg's models (1963, 1967). The brittle plates were made by drying a mixture of sand, plaster and water at a temperature of 90°C (Stephansson, 1971a). A mixture with proportions by weight of 425—450—325 has a density of 1.38 g/cm^3, a Young's modulus of 5500 kg/cm^2 and a tensile strength of 2.4 kg/cm^2. The third type of model material used in the experiments was painter's putty with properties described in a previous section.

Model Ö19. A 5 mm layer of stitching wax was placed in the centrifuge cup with a diameter of almost 20 cm. The source layer had a small bulge for initiating the diapir (Fig. 34). The base layer was covered with a multilayered sequence of painter's putty and brittle plates, the whole column being about 15 mm thick. This model was run in the centrifuge at 2200 g for 210 minutes without diapiric structure becoming visible on the surface. As there was no sign of motion on the surface of the model except for the appearance of fractures it was believed that the model had reached a certain state of equilibrium, so the run was discontinued and the model was analysed.

The long run in the centrifuge had caused

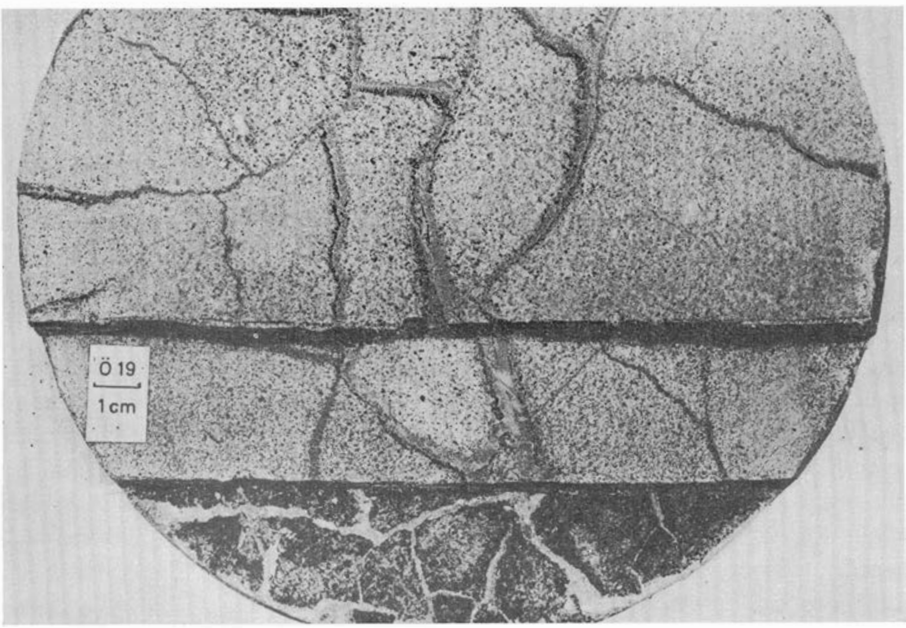

Fig. 35. Model Ö19 after 210 min. run at 2200 g without visible diapirs on the surface of the model. The cracks on the surfaces of brittle plates have been filled with putty from the overlying layer. Notice the resemblance to mud cracks.

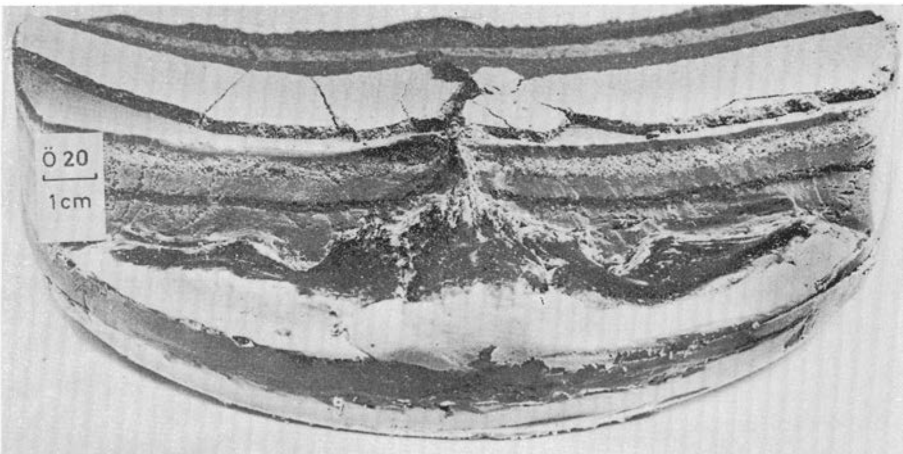

Fig. 36. Model Ö20 after 105 min. run at 2000 g. A ridge has penetrated the overburden. Notice the marked marginal sinks and the bending of the stiff plates.

a certain separation of the oil from the putty giving rise to dark dyeing of the brittle plates. The surfaces of the plates at different levels in the model only showed signs of brittle fracturing and the more plastic putty had penetrated and filled in the open fractures (Fig. 35). The infilling material came from the denser layer of putty situated above each plate. These structures showed a great resemblance to infilled mud cracks.

Model Ö20. To facilitate the formation of a diapir in this model the number of stiff plates were reduced and the height of the diapir-initiating bulge together with the thickness of the adjacent layer of painter's putty were increased (Fig. 34). Now, a slight bulging of the top surface in the centre of the model was obtained after 105 minutes' run in the centrifuge at 2000 g. As the initiating bulge had the form of a ridge this shape was maintained after the run (Fig. 36). We notice the very marked marginal sinks filled with painter's putty, the penetration of stitching wax along the crest of the ridge and the slight bending of the stiff plates.

Model Ö23. This model, originally prepared for a lecture at the VII Nordic Geological Winter meeting in Åbo (Stephansson, 1966), gave the impression of plastic deformation in a brittle material. A cross-section through the model prior to its run in the centrifuge is shown in Fig. 37. A 3 mm layer of wax is overlain by 5 mm of painter's putty followed by a plate of sand-plaster-water mixture 1.5 mm thick. This plate is covered by 25 mm of painter's putty. The model was run in the old centrifuge for 40 minutes at 1750 g.

After removing the top layer of putty a dome with the classical stock shape was revealed (Fig. 38). Here the brittle plate had been penetrated

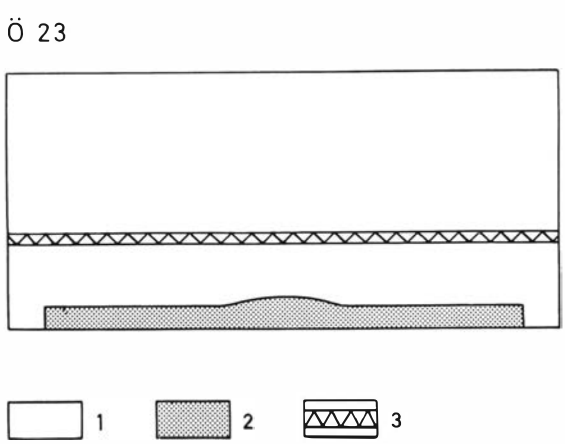

Fig. 37. Cross-section of model Ö23 prior to the run. Model materials: 1, painter's putty; 2, stitching wax; 3, brittle plate of a sand-plaster-water mixture. Diameter of the model 94 mm.

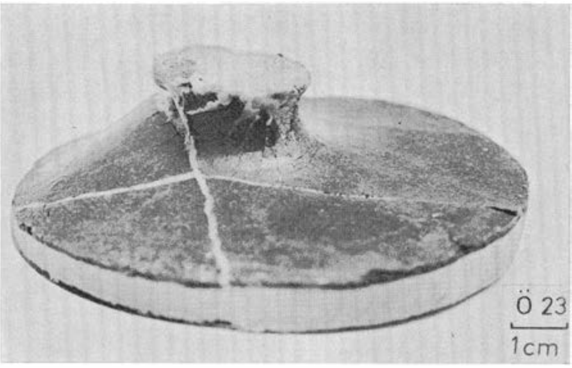

Fig. 38. Model Ö23 after 40 min. run at 1750 g showing brittle or semi-brittle fracturing accompanying plastic deformation of the diapir.

by the wax dome and strongly pushed aside at the border of the trunk. A close examination of the surface of the plate shows an intense fissuring in areas of high deformation. This model well represents brittle or semi-brittle failure accompanying plastic deformation.

ACKNOWLEDGEMENTS

The author is most grateful to Professor H. Ramberg for his encouragement during this investigation and for loan of the computer program for calculating gravity instability.

The stratigraphy of the main ridge at Kvinsgröta was kindly elucidated by Dr. K. Larsson. Doctor B. Dahlman of the Geological Survey of Sweden kindly placed at my disposal density values from the borehole at Segerstad. Thanks are further due to Dr. P. Hudleston, Professor B. Collini and Professor H. Ramberg for reading and critiziting the manuscript.

Mr. A. Lund assisted in the preparation of the models. The drawings were made by Mrs. A. Kaljusaar and Mr. H. Holmström, all at the Institute of Geology, University of Uppsala. Financial support was given by The Swedish Board for Technical Development, grants 5398 and 71-332/U237.

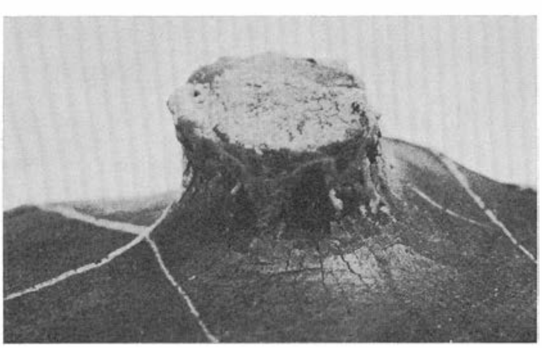

Fig. 39. Detail of model Ö23. Notice the radial cracks at the lower part of the trunk region.

REFERENCES

Arrhenius, S. & Lachmann, R. 1912. Die physikalisch-chemischen Bedingungen bei der Bildungen der Salzlager und ihre Anwendungen auf geologische Probleme. *Geol. Rdsch.* 3, 139—157.

Atwater, G. I. 1967. Origin of diapiric shale structures of South Louisiana (abs.). *Bull. Am. Ass. Petrol. Geol.* 51, p. 452.

Atwater, G. I. & Forman, M. J. 1959. Nature of growth of southern Louisiana salt domes and its effect on petroleum accumulation. *Bull. Am. Ass. Petrol. Geol.* 43, 2592—2622.

Beloussov, V. V. 1962. *Basic Problems in Geotectonics.* Mc Graw-Hill. New York, N.Y. 809 pp.

Bennet, L. C., Jr. 1969. Structural studies of the continental shelf off Washington. *Trans. Am. geophys. Un.* 50, p. 60.

Biot, M. A. & Odé, H. 1965. Theory of gravity instability with variable overburden and compaction. *Geophysics* 30, 213—227.

Bogacz, K., Dzulynski, S., Gradzinski, R. & Kostecka, A. 1968. Origin of crumpled limestone in the Middle Triassic of Poland. *Rocznik Polsk. Towarz. Geol.* 38, 385—397.

Burk, C. A., Ewing, M., Worzel, I. L., Beall, A. O., Jr., Berggren, W. A., Bukry, D., Fischer, A. G. & Pesagno, E. A. 1969. Deep-sea drilling into the Challenger Knoll, central Gulf of Mexico. *Bull. Am. Ass. Petrol. Geol.* 53, 1338—1347.

Daley, B. 1971. Diapiric and other deformational structures in an Oligocene argillaceous limestone. *Sediment Geol.* 6, 29—51.

Dobrin, M. B. 1941. Some quantitative experiments on a fluid salt-dome model and their geological implications. *Trans. Am. geophys. Un.* 22, 528—542.

Dzulynski, S. & Walton, E. K. 1965. *Sedimentary Features of Flysch and Greywackes.* Elsevier, Amsterdam, 274 pp.

Elliot, R. E. 1965. A classification of subaqueous sedimentary structures based on rheological and kinematical parameters. *Sedimentology* 5, 193—209.

Elston, D. P. & Shoemaker, E. M. 1963. Salt anticlines of the Paradox Basin, Colorado and Utah. *Symposium on Salt, Nth. Ohio geol. Soc.* 131—146.

Engelhardt, W. v. 1960. *Der Porenraum der Sedimente.* Springer-Verlag, Berlin, Göttingen, Heidelberg. 207 pp.

Freeman, P. S. 1968. Exposed Middle Tertiary mud diapirs and related features in South Texas. *Am. Ass. Petrol. Geol., Mem.* 8, 162—182.

Friend, P. F. 1965. Fluviatile structures in the Wood Bay Series (Devonian) of Spitsbergen. *Sedimentology* 5, 39—68.

Gidon, P. & Lindström, M. 1965. On the atectonic origin of folds in limestone. *Sedimentology* 4, 315—318.

Gill, W. D. & Kuenen, Ph. H. 1958. Sand volcanoes on slumps in the Carboniferous of County Clare, Ireland. *Q. Jl. geol. soc. Lond.* 113, 441—460.

Gilreath, J. A. 1968. Electric-log characteristics of diapiric shale. *Am. Ass. Petrol. Geol., Mem.* 8, 137—144.

Graff-Petersen, P. 1967. Intraformational deformations and porewater hydrodynamics. *Proc. 7th Intern. Congr. Sedimentol., Reading and Edinburgh 1967* (pages unnumbered).

Griggs, D. T. 1936. Deformation of rocks under high confining pressure. *J. Geol.* 44, 541—577.

— 1939. Creep of rocks. *J. Geol.* 47, 225—251.

Griggs, D. T. & Handin, J. 1960. Observation on fracture and a hypothesis of earthquake. *In* Rock Deformation. *Mem. geol. Soc. Am.* 79, 347—364.

Handin, J. 1968. Experimental evidence for the effect of pore water pressure on the strength and ductility of rocks. *In* R. Riecker (editor): *Rock mechanics seminar,* Air Force Cambridge Res. Lab., Bedford, Mass.

Hardy, H. R. 1959. Time-dependent deformation and failure of geologic materials. *Colo. Sch. Mines Q.* 54, 134—175.

Heard, H. C. 1968. Experimental deformation of rocks and the problem of extrapolation to nature. *In* R. Riecker (editor) *Rock mechanics seminar,* Air Force Cambridge Res. Lab., Bedford, Mass.

Hessland, I. 1955. Studies in the lithogenesis of the Cambrian and Basal Ordovician of the Böda Hamn sequence of strata. *Bull. geol. Instn Univ. Upsala* 35, 35—109.

Higgins, G. E. & Saunders, J. B. 1967. Report on 1964 Chatham Mud Island, Erin Bay, Trinidad, West Indies. *Bull. Am. Ass. Petrol. Geol.* 51, 55—64.

Hubbert, M. K. & Rubey, W. W. 1959. Role of fluid pressure in mechanics of overthrust faulting. *Bull. geol. Soc. Am.* 70, 115—166.

Jaanusson, V. 1961. Discontinuity-surfaces in limestones. *Bull. geol. Instn Univ. Upsala* 40, 221—241.

Kidybinsky, A. 1966. Rheological models of Upper Silesian Carboniferous rocks. *Int. J. Rock Mech. Min. Sci.* 3, 279—306.

Kuenen, Ph. H. 1953. Significant features of graded bedding. *Bull Am. Ass. Petrol. Geol.* 37, 1044—1066.

Larsen, G. & Chilingar, G. V. 1967. *Diagenesis in sediments.* Elsevier Amsterdam. 551 pp.

Lindström, M. 1963. Sedimentary folds and the development of limestone in an Early Ordovician sea. *Sedimentology* 2, 243—292.

— 1971. Vom Angang, Hochstand und Ende eines Epikontinentalmeeres. *Geol. Rdsch.* 60, 419—438.

— 1971. Small-scale domes and piercing-structures in the Lower Ordovician limestones of Oeland (S. E. Sweden). Comment on a paper by W. A. van Wamel. *Koninkl. Nederl. Akad. Wetensch.-Amsterdam, Proc., Ser. B* 74, 93—95.

Magnusson, N. H., Thorslund, P., Brotzen, F., Asklund, B. & Kulling, O. 1962. Beskrivning till karta över Sveriges berggrund. *Sver. geol. Unders. Afh. Ser. Ba* 16, 290 pp.

Martinsson, A. 1958. Deep boring on Gotska Sandön. I The submarine morphology of the Baltic Cambro-Silurian area. *Bull. geol. Instn Univ. Upsala* 38, 11—35.

Morgan, J. P., Coleman, J. M. & Gagliano, S. M. 1968. Mudlumps: diapiric structures in Mississippi delta sediments. *Am. Ass. Petrol. Geol., Mem.* 8, 145—161.

Morgans, W. T. A. & Terry, N. B. 1968. Measurements of the static and dynamic elastic moduli of coal. *Fuel* 37, 201—219.

Musgrave, A. W. & Hicks, W. G. 1968. Outlining shale masses by geophysical methods. *Am. Ass. Petrol. Geol., Mem.* 8, 122—136.

Nettleton, L. L. 1934. Fluid mechanics of salt domes. *Bull. Am. Ass. Petrol. Geol.* 18, 1175—1204.

— 1943. Recent experimental and geophysical evidence of mechanics of salt-dome formation. *Bull. Am. Ass. Petrol. Geol.* 27, 51—63.

Nettleton, L. L. & Elkins, T. A. 1947. Geologic models made from granular materials. *Trans. Am. geophys. Un.* 28, 451—466.

O'Brien, G. D. 1968. Survey of diapirs and diapirism. *Am. Ass. Petrol. Geol., Mem.* 8, 1—9.

Odé, H. 1966. Gravitational instability of a multilayered system of high viscosity. *Ver. K. Ned. Akad. Wet. Reeks* 1, vol. XXIV, No 1, 96 pp.

— 1968. Review of mechanical properties of salt relating to salt-dome genesis. *Am. Ass. Petrol. Geol., Mem.* 8, 53—78.

Omara, S. M. 1964. Diapiric structures in Egypt and Syria. *Bull. Am. Ass. Petrol. Geol.* 48, 1116—1125.

Parker, T. J. & McDowell, A. N. 1955. Model studies of salt-dome tectonics. *Bull. Am. Ass. Petrol. Geol.* 39, 2384—2470.

Price, N. J. 1964. A study of the time-strain behaviour of coal-measure rocks. *Int. J. Rock Mech. Min. Sci.* 1, 277—303.

— 1966. *Fault and joint development in brittle and semi-brittle rock.* Pergamon Press. 176 pp.

Ramberg, H. 1963. Experimental study of gravity tectonics by means of centrifuged models. *Bull. geol. Instn Univ. Upsala* XLII, 1—97.

— 1967a. *Gravity, deformation and the Earth's crust.* Academic Press London. 214 pp.

— 1967b. Model experimentation of the effect of gravity on tectonic processes. *Geophys. J. Roy. Astr. Soc.* 14, 307—329.

— 1968a. Fluid dynamics of layered systems in the field of gravity, a theoretical basis for certain global structures and isostatic adjustment. *Phys. Earth Planet. Interiors* 1, 63—87.

— 1968b. Instability of layered systems in the field of gravity. I and II. *Phys. Earth Planet. Interiors* 1, 427—474.

— 1970. Model studies in relation to intrusion of plutonic bodies. *In* G. Newall & N. Rast (editors), *Mechanism of Igneous Intrusion.* Geol. Journ. Spec. Iss. No 2., 261—286.

— 1972. Inverted density stratification and diapirism in the Earth. (In print).

Rubey, W. W. Hubbert, M. K. 1959. Overthrust belt in geosynclinal area of western Wyoming in light of fluid-pressure hypothesis, pt. 2. *Bull. geol. Soc. Am.* 70, 167—205.

Sanneman, D. 1963. Über Salzstock-Familien in Nordwestdeutschland. *Erdöl-Z,* 11, 3—10.

Scholl, D. W. & Marlow, M. S. 1970. Diapirlike structures in southeastern Bering Sea. *Bull. Am. Ass. Petrol. Geol.* 54, 1644—1650.

Schwarbrick, E. E. 1968. Physical diagenesis; intrusive sediment and connate water. *Sediment. Geol.* 2, 161—175.

Shinn, E. A. 1969. Submarine lithification of Holocene carbonate sediments in the Persian Gulf. *Sedimentology* 5, 109—144.

Shrock, B. R. 1948. *Sequence in layered rocks.* Mc Graw-Hill, New York, N.Y. 507 pp.

Stephansson, O. 1966. Modellstudier av saltdomer. Lecture at VII Nordic Geological Winter Meeting, Åbo, Finland.

— 1967. Bergarternas mekaniska och reologiska egenskaper. Reologisk undersökning av tektoniska modellmaterial — en jämförelse med bergarternas deformationsegenskaper. Fil.lic. thesis Geol. Inst., Univ. Uppsala, 198 pp.

— 1971a. Stability of single openings in horizontally bedded rock. *Eng. Geol.* 5, 5—71.

— 1971. Gravity tectonics on Öland. *Bull. geol. Instn Univ.* Upsala, N.S. 3, 4: 37—78.

Suter, H. H. 1955. Present tectonic activity in Trinidad, B.W.I. *Geol. Rdsch.* 43, 264—265.

Trusheim, F. 1960. Mechanism of salt migration in northern Germany. *Bull. Am. Ass. Petrol. Geol.* 44, 1519—1540.

Wamel, W. A. v. 1970. Small-scale domes and piercing-structures in the Lower Ordovician limestones of Oeland (S.E. Sweden). *Koninkl. Nederl. Akad. Wetensch. — Amsterdam, Proc.*, Ser B 73, 293—304.

Watson, J. A. & Johnson, G. L. 1968. Mediterranean diapiric structures. *Bull. Am. Ass. Petrol. Geol.* 52, 2247—2249.

Wiedenmayer, C. 1950. Zur Geologie des Bologneser Apennins zwischen Reno- und Idice-Tal. *Eclog. geol. Helv.* 43, 115—144.

Printed by Ekenäs Tryckeri Ab, Ekenäs, Finland March, 1972.